arXiv:quant-ph/0211042v1 8 Nov 2002

Constructive control of quantum systems using factorization of unitary operators

S. G. Schirmer

Quantum Processes Group and Department of Applied Maths, The Open University, Milton Keynes, MK7 6AA, United Kingdom

Andrew D. Greentree

Quantum Processes Group and Department of Physics and Astronomy, The Open University, Milton Keynes, MK7 6AA, United Kingdom

Viswanath Ramakrishna

Center for Signals, Systems and Telecommunications and Dept of Mathematical Sciences , EC 35, University of Texas at Dallas, Richardson, Texas 75083, USA

Herschel Rabitz

Department of Chemistry, Frick Laboratories, Princeton University, Princeton, NJ 08544, USA

E-mail: `s.g.schirmer@open.ac.uk`, `a.d.greentree@open.ac.uk`, `vish@utdallas.edu`, `hrabitz@princeton.edu`

Abstract. We demonstrate how structured decompositions of unitary operators can be employed to derive control schemes for finite-level quantum systems that require only sequences of simple control pulses such as square wave pulses with finite rise and decay times or Gaussian wavepackets. To illustrate the technique, it is applied to find control schemes to achieve population transfers for pure-state systems, complete inversions of the ensemble populations for mixed-state systems, create arbitrary superposition states and optimize the ensemble average of dynamic observables.

PACS numbers: 03.65.Bz

1. Introduction

The ability to control quantum-mechanical systems is an essential prerequisite for many novel applications that require the manipulation of atomic and molecular quantum states [1]. Among the important applications of current interest are quantum state engineering [2], control of chemical reactions [3, 4, 5, 6, 7], control of molecular motion [8], selective vibrational excitation of molecules [9], control of rotational coherence in linear molecules [8], photo-dissociation [10], laser cooling of internal molecular degrees of freedom [11, 12], and quantum computation [13, 14, 15, 16, 17].

Due to the wide range of applications, the immediate aims of quantum control may vary. However, the control objective can usually be classified as one of the following:

(i) To steer the system from its initial state to a target state with desired properties,

(ii) To maximize the expectation value or ensemble average of a selected observable,

(iii) To achieve a certain evolution of the system.

Despite the apparent dissimilarity, these control objectives are closely related. Indeed, (i) is a special case of (ii) in which the observable is the projector onto the subspace spanned by the target state. (ii) is a special case of (iii), where we attempt to find an evolution operator that maximizes the expectation value of the selected observable either at a specific target time or at some time in the future. Hence, one of the central problems of quantum control is to achieve a desired evolution of the system by applying external control fields, and the primary challenge is to find control pulses (or sequences of such pulses) that are feasible from a practical point of view and effectively achieve the control objective.

Many control strategies for quantum systems have been proposed. Selective excitation of energy eigenstates, for instance, can be achieved using light-induced potentials and adiabatic passage techniques [18, 19, 20, 21], which have the advantage of being relatively insensitive to perturbations of the control fields and Doppler shifts arising from atomic or molecular motion [22, 23]. Efficient numerical algorithms based on optimal control techniques have been developed to address problems such as optimization of observables for pure-state [24, 25, 26] and mixed-state quantum systems [27, 28]. Quantum feedback control using weak measurements or continuous state estimation has been applied to quantum state control problems [29, 30, 31, 32, 33, 34]. Learning control based on genetic or evolutionary algorithms [35, 36, 37, 38, 39, 40] has been a useful tool for quantum control, especially for complex problems for which accurate models are not available and in experimental settings [41, 42]. Other approaches based on local control techniques [43] or a hydrodynamical formulation [44] have been suggested as well, and this list is not exhaustive.

In this paper we pursue an alternative, constructive approach to address the problem of control of non-dissipative quantum systems. Note that although real atomic or molecular systems are subject to dissipative processes due to the finite lifetimes of the excited states, etc., we can treat these systems as non-dissipative if we ensure that

the time needed to complete the control process is *significantly* less than the relaxation times. The technique we develop is based on explicit generation of unitary operators using Lie group decompositions. Similar techniques have been applied to the problem of controlling two-level systems [45, 46] and especially particles with spin [47, 48]. Here we employ decompositions of the type discussed in [49] to derive constructive control schemes for N-level systems. We use the rotating wave approximation (RWA) and require that *each* allowed transition is *selectively* addressable, for example by applying a field of the appropriate frequency, or by appropriate selection rules depending on the field polarization. This means we must be able to ensure that each control pulse drives a single transition only, and that its effect on all other transitions is negligible. These assumptions limit the applicability of this approach to systems for which selective excitation of individual transitions is feasible such as atomic or molecular systems with well-separated transition frequencies or particles in anharmonic potentials. Certain other factors such as Doppler shifts and inhomogeneous or homogeneous broadening must also be taken into account, and may require special consideration in specific circumstances.

However, for systems that satisfy the necessary conditions, the proposed technique has some very attractive features. It is constructive and can be used to solve a variety of control problems ranging from common problems with well-known solutions such as population transfer between energy eigenstates to novel problems such as preparation of arbitrary superposition states or optimization of observables for N-level systems. Moreover, although the control schemes derived using this technique depend on the effective areas, and to a lesser extent, phases of the control pulses, the pulse *shapes* are flexible, which implies that the control objective can be achieved using control pulses that are convenient from a practical point of view such as square wave pulses with finite rise and decay times (SWP) or Gaussian wavepackets (GWP). SWP are a realistic approximation of bang-bang controls, which play an important role in control theory and have been shown to be crucial for time-optimal control [50]. Since both SWP and GWP can in principle be derived from continuous-wave (CW) lasers using Pockel cells or other intensity modulating devices, this also opens the possibility for control of certain quantum systems using CW lasers, rather than more complex pulsed laser systems and pulse-shaping techniques.

2. Mathematical and physical framework

We consider a non-dissipative quantum system with a discrete, finite energy spectrum such as a generic N-level atom, molecule or particle in an (anharmonic) potential. The free evolution of the system is governed by the Schrodinger equation and determined by its internal Hamiltonian $\hat{H}_0$, whose spectral representation is

$$\hat{H}_0 = \sum_{n=1}^{N} E_n |n\rangle\langle n|, \tag{1}$$

where E_n are the energy levels and $|n\rangle$ the corresponding energy eigenstates of the system, which satisfy the stationary Schrodinger equation

$$\hat{H}_0|n\rangle = E_n|n\rangle, \quad 1 \leq n \leq N. \tag{2}$$

Although this assumption is not required, we shall assume for simplicity that the energy levels E_n are ordered in an increasing sequence, $E_1 < E_2 < \cdots < E_N$, where $N < \infty$ is the dimension of the Hilbert space of the system, and that the eigenstates $\{|n\rangle : n = 1, \ldots, N\}$ form a complete orthonormal set.

The application of external control fields perturbs the system and gives rise to a new Hamiltonian $\hat{H} = \hat{H}_0 + \hat{H}_I$, where $\hat{H}_I$ is an interaction term. If we apply a field

$$f_m(t) = 2A_m(t)\cos(\omega_m t + \phi_m) = A_m(t)\left[e^{\mathrm{i}(\omega_m t+\phi_m)} + e^{-\mathrm{i}(\omega_m t+\phi_m)}\right] \tag{3}$$

which is resonant with the frequency ω_m corresponding to the transition $|m\rangle \to |m+1\rangle$, and the pulse envelope $2A_m(t)$ is slowly varying with respect to the frequency ω_m, then the rotating wave approximation (RWA) leads to the following interaction term

$$\hat{H}_m(f_m) = A_m(t)d_m\left[e^{\mathrm{i}(\omega_m t+\phi_m)}|m\rangle\langle m+1| + e^{-\mathrm{i}(\omega_m t+\phi_m)}|m+1\rangle\langle m|\right] \tag{4}$$

provided that (a) there are no other transitions with the same frequency ω_m and (b) off-resonant effects are negligible. Note that the latter assumption is generally valid only if the Rabi frequency Ω_m of the driven transition is considerably less than the minimum detuning from off-resonant transitions $\Delta\omega_{min}$, i.e.,

$$\max_t[\Omega_m(t)] = \max_t[2A_m(t)d_m/\hbar] \ll \Delta\omega_{min}, \tag{5}$$

where d_m is the dipole moment of the transition $|m\rangle \to |m+1\rangle$.

The evolution of the controlled system is determined by the operator $\hat{U}(t)$, which satisfies the Schrodinger equation

$$\mathrm{i}\hbar\frac{d}{dt}\hat{U}(t) = \left\{\hat{H}_0 + \sum_{m=1}^{M}\hat{H}_m[f_m(t)]\right\}\hat{U}(t) \tag{6}$$

and the initial condition $\hat{U}(0) = \hat{I}$, where $\hat{I}$ is the identity operator.

3. Constructive control using Lie group decompositions

Our aim is to achieve a certain evolution of the system by applying a sequence of simple control pulses. Concretely, we seek to dynamically realize a desired unitary operator $\hat{U}(t)$ at a certain target time $t = T$. In some cases, we may not wish to specify a target time in advance, in which case we attempt to achieve the control objective at some later time $T > 0$.

To solve the problem of finding the right sequence of control pulses, we apply the interaction picture decomposition of the time-evolution operator $\hat{U}(t)$,

$$\hat{U}(t) = \hat{U}_0(t)\hat{U}_I(t), \tag{7}$$

where $\hat{U}_0(t)$ is the time-evolution operator of the unperturbed system

$$\hat{U}_0(t) = \exp\left(-\mathrm{i}\hat{H}_0 t/\hbar\right) = \sum_{n=1}^{N} e^{-\mathrm{i}E_n t/\hbar}|n\rangle\langle n| \tag{8}$$

and $\hat{U}_I(t)$ comprises the interaction with the control fields. To obtain a dynamical law for the interaction operator $\hat{U}_I(t)$, we note that inserting

$$\begin{aligned}\mathrm{i}\hbar\frac{d}{dt}\hat{U}(t) &= \hat{H}_0\hat{U}_0(t)\hat{U}_I(t) + \mathrm{i}\hbar\hat{U}_0(t)\frac{d}{dt}\hat{U}_I(t)\\ \hat{H}\hat{U}(t) &= \hat{H}_0\hat{U}_0(t)\hat{U}_I(t) + \sum_{m=1}^{M}\hat{H}_m[f_m(t)]\hat{U}_0(t)\hat{U}_I(t)\end{aligned}$$

into the Schrodinger equation (6) gives

$$\mathrm{i}\hbar\frac{d}{dt}\hat{U}_I(t) = \hat{U}_0(t)^\dagger\left\{\sum_{m=1}^{M}\hat{H}_m[f_m(t)]\right\}\hat{U}_0(t)\hat{U}_I(t). \tag{9}$$

Applying (8) and the rotating wave approximation Hamiltonian (4) to this equation leads after some simplification (see Appendix A) to

$$\frac{d}{dt}\hat{U}_I(t) = \sum_{m=1}^{M} A_m(t)d_m/\hbar\left(\hat{x}_m\sin\phi_m - \hat{y}_m\cos\phi_m\right)\hat{U}_I(t) \tag{10}$$

where we set $\hat{e}_{m,n} = |m\rangle\langle n|$ and define

$$\hat{x}_m = \hat{e}_{m,m+1} - \hat{e}_{m+1,m}, \qquad \hat{y}_m = \mathrm{i}(\hat{e}_{m,m+1} + \hat{e}_{m+1,m}). \tag{11}$$

Hence, if we apply a control pulse $f_k(t) = 2A_k(t)\cos(\omega_m t + \phi_k)$ which is resonant with the transition frequency ω_m for a time period $t_{k-1} \le t \le t_k$ (and no other fields are applied during this time period) then we have

$$\hat{U}_I(t) = \hat{V}_k(t)\hat{U}_I(t_{k-1}), \tag{12}$$

where the operator $\hat{V}_k(t)$ is

$$\hat{V}_k(t) = \exp\left[\frac{d_m}{\hbar}\int_{t_{k-1}}^{t} A_k(t')\,dt'\left(\hat{x}_m\sin\phi_k - \hat{y}_m\cos\phi_k\right)\right]. \tag{13}$$

Thus, if we partition the time interval $[0,T]$ into K subintervals $[t_{k-1},t_k]$ such that $t_0 = 0$ and $t_K = T$, and apply a sequence of non-overlapping control pulses, each resonant with one of the transition frequencies $\omega_m = \omega_{\sigma(k)}$, then

$$\hat{U}(T) = \hat{U}_0(T)\hat{U}_I(T) = e^{-\mathrm{i}\hat{H}_0 T/\hbar}\hat{V}_K\hat{V}_{K-1}\cdots\hat{V}_1, \tag{14}$$

where the factors $\hat{V}_k$ are

$$\hat{V}_k = \exp\left[\frac{d_{\sigma(k)}}{\hbar}\int_{t_{k-1}}^{t_k} A_k(t)\,dt\left(\hat{x}_{\sigma(k)}\sin\phi_k - \hat{y}_{\sigma(k)}\cos\phi_k\right)\right]. \tag{15}$$

$2A_k(t)$ is the envelope of the kth pulse and σ is a mapping from the index set $\{1,\ldots,K\}$ to the control index set $\{1,\ldots,M\}$ that determines which of the control fields is active for $t \in [t_{k-1},t_k]$.

It has been shown [49] that any unitary operator $\hat{U}$ can be decomposed into a product of operators of the type $\hat{V}_k$ and a phase factor $e^{\mathrm{i}\Gamma} = \det\hat{U}$, i.e., there exists a

positive real number Γ, real numbers C_k and ϕ_k for $1 \leq k \leq K$, and a mapping σ from the index set $\{1, \ldots, K\}$ to the control-sources index set $\{1, \ldots, M\}$ such that

$$\hat{U} = e^{\mathrm{i}\Gamma} \hat{V}_K \hat{V}_{K-1} \cdots \hat{V}_1, \tag{16}$$

where the factors are

$$\hat{V}_k = \exp\left[C_k(\hat{x}_{\sigma(k)} \sin\phi_k - \hat{y}_{\sigma(k)} \cos\phi_k)\right]. \tag{17}$$

This decomposition of the target operator into a product of generators of the dynamical Lie group determines the sequence in which the fields are to be turned on and off. A general algorithm to determine the Lie group decomposition for an arbitrary operator $\hat{U}$ is described in Appendix B.

Note that in many cases the target operator $\hat{U}$ is unique only up to phase factors, i.e., two unitary operators $\hat{U}_1$ and $\hat{U}_2$ in $U(N)$ are equivalent if there exist values $\theta_n \in [0, 2\pi]$ for $1 \leq n \leq N$ such that

$$\hat{U}_2 = \hat{U}_1 \left(\sum_{n=1}^{N} e^{\mathrm{i}\theta_n} |n\rangle\langle n|\right) \tag{18}$$

where $|n\rangle$ are the energy eigenstates. For instance, if the initial state of the system is an arbitrary ensemble of energy eigenstates

$$\hat{\rho}_0 = \sum_{n=1}^{N} w_n |n\rangle\langle n|, \tag{19}$$

where w_n is the initial population of state $|n\rangle$ satisfying $0 \leq w_n \leq 1$ and $\sum_{n=1}^{N} w_n = 1$, then we have

$$\hat{U}_2 \hat{\rho}_0 \hat{U}_2^\dagger = \hat{U}_1 \left(\sum_{n=1}^{N} |n\rangle e^{\mathrm{i}\theta_n} w_n e^{-\mathrm{i}\theta_n} \langle n|\right) \hat{U}_1^\dagger = \hat{U}_1 \hat{\rho}_0 \hat{U}_1^\dagger$$

i.e., the phase factors $e^{\mathrm{i}\theta_n}$ cancel. Thus, if the initial state of the system is an ensemble of energy eigenstates, which of course includes trivial ensembles such as pure energy eigenstates, then we only need to find a Lie group decomposition of the target operator $\hat{U}$ modulo phase factors, i.e., it suffices to find matrices $\hat{V}_k$ such that

$$\hat{U} \left(\sum_{n=1}^{N} e^{\mathrm{i}\theta_n} |n\rangle\langle n|\right) = \hat{V}_K \hat{V}_{K-1} \cdots \hat{V}_1. \tag{20}$$

Note that decomposition modulo phase factors, when sufficient, is more efficient since it requires in general up to $2(N-1)$ fewer steps than the general decomposition algorithm. See Appendix B for details.

4. Choice of pulse envelopes and pulse lengths

Comparing equations (15) and (17) shows that

$$\frac{d_{\sigma(k)}}{\hbar} \int_{t_{k-1}}^{t_k} A_k(t)\, dt = C_k \qquad \forall k, \tag{21}$$

i.e., the effective pulse area of the kth pulse is $2C_k$ where C_k is the constant in decomposition (16). However, the decomposition does not fix the pulse shapes, i.e.,

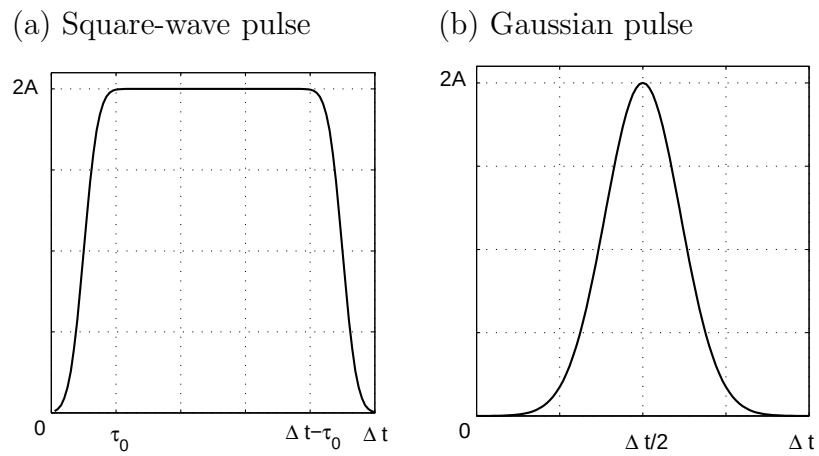

Figure 1. Square wave pulse of length Δt_k with rise and decay time τ_0 and amplitude $2A_k$ (a) and Gaussian wavepacket with $q_k = \frac{4}{\Delta t_k}$ and peak amplitude $2A_k$ (b).

we can choose pulse shapes that are convenient from a practical point of view such as square wave pulses with finite rise and decay times (SWP) and Gaussian wavepackets (GWP), which can easily be produced in the laboratory. For instance, in the optical regime both SWP and GWP can be created using a combination of continuous-wave lasers and Pockel cells or other intensity modulating devices. Moreover, GWP are naturally derived from most pulsed laser systems.

4.1. Square wave pulses

The pulse area of an ideal square wave pulse of amplitude $2A_k$ and length Δt_k is $2A_k\Delta t_k$. In order to accurately determine the pulse area of a realistic square wave pulse, however, we must take into account the finite rise and decay time τ_0 of the pulse. We can model the pulse envelopes of realistic SWP [see figure 1 (a)] mathematically using

$$2A_k(t) = A_k \left\{2 + \mathrm{erf}\left[4(t-\tau_0/2)/\tau_0\right] - \mathrm{erf}\left[4(t-\Delta t+\tau_0/2)/\tau_0\right]\right\} \tag{22}$$

where $\mathrm{erf}(x)$ is the error function

$$\mathrm{erf}(x) = \frac{2}{\sqrt{\pi}}\int_0^x e^{-t^2}\,dt.$$

Although this envelope function may appear complicated, it can easily be checked that the area bounded by this function and $t_{k-1} \leq t \leq t_k$ equals the area of a rectangle of width $\Delta t_k - \tau_0$ and height $2A_k$. Thus, the pulse area $\int_{\Delta t_k} 2A_k(t)\,dt$ of a realistic square wave pulse is $2A_k(\Delta t_k - \tau_0)$, and equation (21) shows that the amplitude of the pulse is determined by

$$A_k = \frac{1}{\Delta t_k - \tau_0} \times \frac{\hbar}{d_{\sigma(k)}} \times C_k = \frac{\hbar C_k}{(\Delta t_k - \tau_0)d_{\sigma(k)}}, \tag{23}$$

where $d_{\sigma(k)}$ is the dipole moment of the driven transition.

To ensure selective excitation, the contribution of Fourier components with $\Delta\omega \geq \Delta\omega_{min}$ must be negligeable. Noting that the Fourier transform of an ideal SWP ($\tau_0 = 0$) of length Δt_k and amplitude $2A_k$ is

$$F(\Delta\omega) = 2A_k\sqrt{\frac{2}{\pi}}\frac{\sin(\frac{1}{2}\Delta t_k\Delta\omega)}{\Delta\omega}, \tag{24}$$

where $\Delta\omega$ is the detuning from the pulse frequency ω_m, shows that $F(0) = \sqrt{\frac{2}{\pi}}A_k\Delta t_k$ and

$$\frac{F(\Delta\omega)}{F(0)} = \frac{\sin(\frac{1}{2}\Delta t_k\Delta\omega)}{\frac{1}{2}\Delta t_k\Delta\omega},$$

i.e., $\frac{F(\Delta\omega)}{F(0)} \ll 1$ if $\Delta t_k\Delta\omega \gg 1$. Thus, contributions from Fourier components with $\Delta\omega \geq \Delta\omega_{min}$ will be negligible if $\Delta t_k \gg \Delta\omega_{min}^{-1}$.

Furthermore, noting that $C_k \leq \frac{\pi}{2}$, the peak Rabi frequency for a square wave pulse of length Δt_k with rise and decay time τ_0 is

$$\max_{t_{k-1}\leq t\leq t_k}\left[2A_k(t)d_{\sigma(k)}/\hbar\right] = \frac{2C_k}{\Delta t_k - \tau_0} \leq \frac{\pi}{\Delta t_k - \tau_0}. \tag{25}$$

Hence, the Rabi frequency and the amplitude of the pulse can be adjusted by changing the pulse length Δt_k, which allows us to ensure that (5) is satisfied, and enforce laboratory constraints on the strengths of the control fields.

We can also give an estimate of the time required to implement arbitrary unitary operators given certain bounds on the field strength. If the maximum strength of the field produced by the mth laser is $A_{m,max}$, i.e, $f_m(t) = 2A_m(t)\cos(\omega_m t + \phi_m) \leq A_{m,max}$ then the time required to perform a rotation by C_k on the transition $|m\rangle \to |m+1\rangle$ using a SWP with rise and decay time τ_0 is

$$\Delta t_m^{SWP} = \frac{2C_k\hbar}{A_{m,max}d_m} + \tau_0 \leq \frac{\pi\hbar}{A_{m,max}d_m} + \tau_0. \tag{26}$$

Appendix B shows that any unitary operator $\hat{U}$ can be generated up to equivalence (18) by performing at most $N-m$ rotations by $C \leq \frac{\pi}{2}$ on each transition $|m\rangle \to |m+1\rangle$ for $m = 1, 2, \ldots, N-1$. Hence, any unitary operator can be implemented up to equivalence using SWP of amplitude $A_{m,max}$ in at most time T, where

$$T = \sum_{m=1}^{N-1}\max(\Delta t_m^{SWP})(N-m) = \sum_{m=1}^{N-1}\left(\frac{\pi\hbar}{A_{m,max}d_m} + \tau_0\right)(N-m). \tag{27}$$

Since two additional rotations on each transition are required to generate $\hat{U}$ exactly, the latter can be accomplished in time $T' \geq \sum_{m=1}^{N-1}\max(\Delta t_m^{SWP})(N-m+2)$.

4.2. Gaussian wavepackets

To model a Gaussian wavepacket [see figure 1 (b)] of peak amplitude $2A_k$ centered at $t_k^* = t_{k-1} + \frac{1}{2}\Delta t_k$, we choose the pulse envelope

$$2A_k(t) = 2A_k\exp\left[-q_k^2(t - \Delta t_k/2 - t_{k-1})^2\right]. \tag{28}$$

The constant q_k determines the width of the wavepacket. The pulse area of a Gaussian wavepacket is $\sqrt{\pi}/q_k$ provided that the time interval Δt_k is large enough to justify the assumption

$$\int_{t_{k-1}}^{t_k} \exp\left[-q_k^2(t-\Delta t_k/2-t_{k-1})^2\right]\, dt \approx \int_{-\infty}^{+\infty} e^{-q^2\tau^2}\, d\tau = \frac{\sqrt{\pi}}{q_k}.$$

In the following we choose $q_k = 4/\Delta t_k$, which guarantees that over 99% of the kth pulse is contained in the control interval $[t_{k-1}, t_k]$ since

$$\int_{-\Delta t_k/2}^{\Delta t_k/2} e^{-q_k^2 t^2}\, dt = \frac{\sqrt{\pi}}{q_k}\mathrm{erf}(q_k\Delta t_k/2)$$

and $\mathrm{erf}(2) = 0.995322$. Thus, (21) shows that the peak amplitude $2A_k$ of the GWP is determined by

$$A_k = \frac{q_k}{\sqrt{\pi}} \times \frac{\hbar}{d_{\sigma(k)}} \times C_k = \frac{4\hbar C_k}{\sqrt{\pi}\Delta t_k d_{\sigma(k)}}. \tag{29}$$

Again, to ensure selective excitation, the contribution of Fourier components with $\Delta\omega \geq \Delta\omega_{min}$ must be negligeable. Noting that the Fourier transform of a Gaussian wavepacket with $q_k = 4/\Delta t_k$ and amplitude $2A_k$ is

$$F(\Delta\omega) = \frac{2A_k}{\sqrt{2}q_k}\exp\left[-\frac{\Delta\omega^2}{4q_k^2}\right] = \frac{\Delta t_k A_k}{2\sqrt{2}}\exp(-\Delta\omega^2\Delta t_k^2/16) \tag{30}$$

where $\Delta\omega$ is the detuning from the pulse frequency ω_m, shows that

$$\frac{F(\Delta\omega)}{F(0)} = \exp(-\Delta\omega^2\Delta t_k^2/16)$$

i.e., $\frac{F(\Delta\omega)}{F(0)} \ll 1$ if $\Delta t_k\Delta\omega \gg 4$. Thus, contributions from Fourier components with $\Delta\omega \geq \Delta\omega_{min}$ will be negligible if $\Delta t_k \gg 4\Delta\omega_{min}^{-1}$.

Furthermore, noting that $C_k \leq \frac{\pi}{2}$, the peak Rabi frequency for a Gaussian pulse of length Δt_k with $q_k = 4/\Delta t_k$ is

$$\max_{t_{k-1}\leq t\leq t-k}\left[2A_k(t)d_{\sigma(k)}/\hbar\right] = \frac{8C_k}{\sqrt{\pi}\Delta t_k} \leq \frac{4\sqrt{\pi}}{\Delta t_k}. \tag{31}$$

Hence, the Rabi frequency can again be adjusted by changing the pulse length Δt_k, which allows us to ensure that (5) is satisfied and enforce laboratory constraints on the strengths of the control fields.

Again, we can give an estimate of the time required to implement arbitrary unitary operators given certain bounds on the field strength. If the maximum strength of the field produced by the mth laser is $A_{m,max}$, i.e, $f_m(t) = 2A_m(t)\cos(\omega_m t + \phi_m) \leq A_{m,max}$ then the time required to perform a rotation by C_k on the transition $|m\rangle \to |m+1\rangle$ using GWP with $q_k = 4/\Delta t_k$ is

$$\Delta t_m^{GWP} = \frac{8C_k\hbar}{\sqrt{\pi}A_{m,max}d_m} \leq \frac{4\sqrt{\pi}\hbar}{A_{m,max}d_m}. \tag{32}$$

Since any unitary operator $\hat{U}$ can be generated up to equivalence (18) by performing at most $N-m$ rotations by $C_k \leq \frac{\pi}{2}$ on each transition $|m\rangle \to |m+1\rangle$ for $m = 1, 2, \ldots, N-1$,

the time required to implement $\hat{U}$ up to equivalence using GWP of (peak) amplitude $A_{m,max}$ is at most

$$T = \sum_{m=1}^{N-1} \max(\Delta t_m^{GWP})(N-m) = \sum_{m=1}^{N-1} \left(\frac{4\sqrt{\pi}\hbar}{A_{m,max} d_m} \right) (N-m). \tag{33}$$

Since two additional rotations on each transition are required to generate $\hat{U}$ exactly, the latter can be accomplished in time $T' \geq \sum_{m=1}^{N-1} \max(\Delta t_m^{GWP})(N-m+2)$.

5. Physical systems used for illustration

In the following sections we shall apply these results to various control problems. For numerical illustrations of our control schemes, we shall consider

(i) a four-level model of the electronic states of Rubidium (^{87}Rb)

(ii) a four-level Morse oscillator model of the vibrational modes of hydrogen fluoride.

For Rubidium (^{87}Rb) we consider four electronic states, which we label as follows: $|1\rangle = |5S_{1/2}\rangle$, $|2\rangle = |5P_{3/2}\rangle$, $|3\rangle = |4D_{1/2}\rangle$ and $|4\rangle = |6P_{3/2}\rangle$, where $|1\rangle$ is the ground state. Figure 2 (a) shows the coupling diagram with transition frequencies and dipole moments.

For hydrogen fluoride (HF) we use the Morse oscillator model given in [51]. The energy levels corresponding to the vibrational states $|n\rangle$ are

$$E_n = \hbar\omega_0 \left(n - \tfrac{1}{2}\right) \left[1 - \tfrac{B}{2}(n - \tfrac{1}{2})\right]$$

where $\omega_0 = 0.78 \times 10^{15}$ Hz and $B = 0.0419$. The frequencies for transitions between adjacent energy levels are $\omega_n = \hbar\omega_0(1 - Bn)$ and the corresponding transition dipole moments are $d_n = p_0\sqrt{n}$ with $p_0 = 3.24 \times 10^{-31}$ C m, which leads to the values shown in figure 2 (b). Although there are 24 bound vibrational states for this model, we only consider the four lowest vibrational modes $n = 1, 2, 3, 4$, where $|1\rangle$ is the ground state.

Since we have made several approximations in developing our control approach using Lie group decompositions, we must ensure that the assumptions we made are valid for the systems we consider:

(i) No two transitions have the same transition frequency.‡

(ii) Dissipative effects are negligible.

(iii) The effect of the pulse on off-resonant transitions is negligible.

Note that both models satisfy hypothesis (1). Furthermore, the main source of dissipation for both systems is spontaneous emission. Thus, dissipative effects will be negligible provided that the control pulses are much shorter than the lifetimes of the excited states. Since the lifetimes of the excited electronic states for ^{87}Rb are 28, 90 and 107 ns, respectively, hypothesis (ii) will be satisfied for control pulses in the sub-nanosecond regime. Similarly for HF.

Hypothesis (iii) will be satisfied provided that:

‡ Assumption (1) can be relaxed if we can distinguish transitions with the same transition frequency by other means, e.g., by using fields with different polarizations.

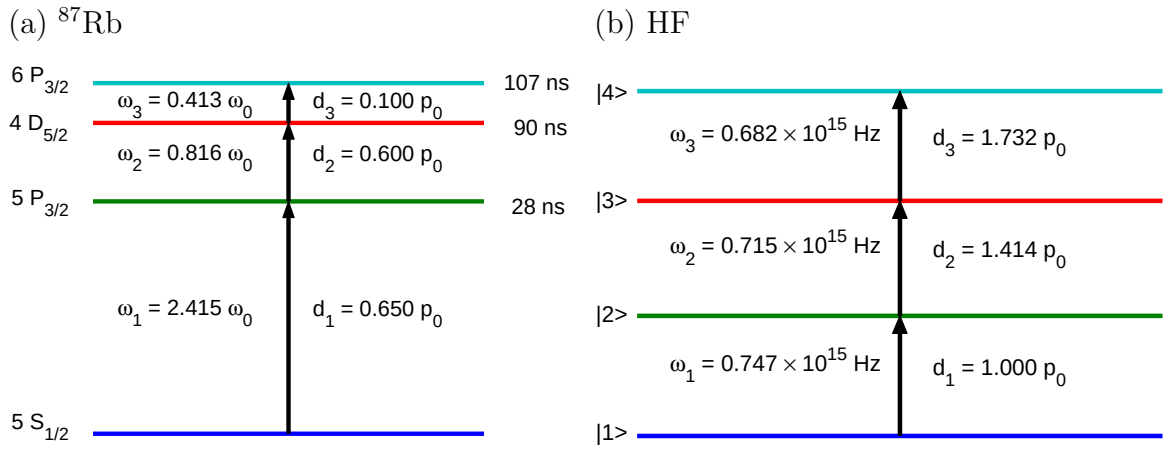

Figure 2. Transition diagram for Rubidium (a) and hydrogen fluoride (b). For ^{87}Rb the constant $\omega_0 = 10^{15}$ Hz and the electric dipole moment unit is $p_0 = 4.89 \times 10^{-29}$ C m. For HF the electric dipole moment unit is $p_0 = 3.24 \times 10^{-31}$ C m.

(a) The Fourier spectrum of the pulse does not overlap with other transition frequencies, i.e., the frequency dispersion of the pulse is less than the minimum detuning from off-resonant transitions.

(b) Equation (5) holds, i.e., the Rabi frequency of each driven transition is much smaller than the minimum detuning from off-resonant transitions.

Since the minimum detuning from off-resonant transitions is $\Delta\omega_{min} \approx 4 \times 10^{14}$ Hz for ^{87}Rb and $\Delta\omega_{min} \approx 3.27 \times 10^{13}$ Hz for HF, the pulse length Δt_k should be at least 10^{-12} and 10^{-11} seconds, respectively, to ensure that the frequency dispersion of the pulse is sufficiently small. Moreover, inserting the values for $\Delta\omega_{min}$ as well as (25) and (31), respectively, into equation (5) shows again that we must choose the pulse lengths such that $\Delta t_k \gg 10^{-14}$ s for ^{87}Rb and $\Delta t_k \gg 10^{-13}$ s for HF to ensure that the second condition above is met. In the following, we shall choose $\Delta t_k = 2 \times 10^{-10}$ seconds (200 ps) for all pulses, which ensures that both hypotheses (ii) and (iii) are met for both ^{87}Rb and HF. Moreover, such pulses are also experimentally realizable.

Note that the energy levels for ^{87}Rb are multiply degenerate due to hyperfine and other effects. Since the detuning between the $F = 1$ and $F = 2$ sublevels of the $5S_{1/2}$ ground state is rather large (6.8 GHz), we may wish to be precise and choose $|1\rangle = |5S_{1/2}, F = 1\rangle$, for instance, but we shall generally ignore the hyperfine energy level structure here. For the cases we consider in this paper, this is justified since the frequency differences between the hyperfine levels (except for the ground state) are on the order of several hundred MHz or less, which corresponds to detunings of $\Delta\omega \leq 10^8$ Hz, which we cannot resolve with 200 ps pulses for reasons outlined above.

6. Population transfer $|1\rangle \to |N\rangle$ for a N-level system

We shall first apply the decomposition technique described above to the rather elementary control problem of population transfer between energy eigenstates to better illustrate the technique. Concretely, we consider the problem of transferring the population of the ground state $|1\rangle$ to the excited state $|N\rangle$ by applying a sequence of control pulses, each resonant with one of the transitions frequencies ω_m. It can easily be verified that any evolution operator $\hat{U}$ of the form

$$\hat{U} = \left(\begin{array}{c|c} \mathbf{0} & A_{N-1} \\ \hline e^{\mathrm{i}\theta} & \mathbf{0} \end{array}\right), \tag{34}$$

where A_{N-1} is an arbitrary unitary $(N-1)\times(N-1)$ matrix, $e^{\mathrm{i}\theta}$ is an arbitrary phase factor and $\mathbf{0}$ is a vector whose $N-1$ elements are 0, achieves the control objective since

$$\left(\begin{array}{c|c} \mathbf{0} & A_{N-1} \\ \hline e^{\mathrm{i}\theta} & \mathbf{0} \end{array}\right)\left(\begin{array}{c} 1 \\ \mathbf{0} \end{array}\right) = \left(\begin{array}{c} \mathbf{0} \\ e^{\mathrm{i}\theta_N} \end{array}\right)$$

and thus the population of state $|N\rangle$ is equal to $\sqrt{e^{-\mathrm{i}\theta_N} e^{\mathrm{i}\theta_N}} = 1$ after application of $\hat{U}$. Next, we observe that setting

$$\hat{U} = \hat{U}_0(T)\hat{U}_I, \quad \hat{U}_I = \hat{V}_{N-1}\hat{V}_{N-2}\cdots\hat{V}_1, \tag{35}$$

where the factors are

$$\begin{aligned} \hat{V}_m &= \exp\left[\frac{\pi}{2}\left(\hat{x}_m \sin\phi_m - \hat{y}_m \cos\phi_m\right)\right] \\ &= -\,\mathrm{i}(e^{\mathrm{i}\phi_m}\hat{e}_{m,m+1} + e^{-\mathrm{i}\phi_m}\hat{e}_{m+1,m}) + \sum_{n\neq m,m+1} \hat{e}_{n,n} \end{aligned} \tag{36}$$

for $1 \le m \le N-1$, always leads to a $\hat{U}$ of the form (34), independent of the initial pulse phases ϕ_m.

The factorization (35) corresponds to a sequence of $N-1$ control pulses in which the mth pulse is resonant with the frequency ω_m of the transition $|m\rangle \to |m+1\rangle$ and has effective pulse area π. Thus, the solution obtained using the decomposition technique is an intuitive sequence of π-pulses designed to transfer the population step by step to the target level.

The results of illustrative computations for the four-level ^{87}Rb system introduced above are shown in figure 3. The top graphs show the pulse sequence for square wave pulses (a) and Gaussian control pulses (b). The corresponding evolution of the energy-level populations shows that the populations of the intermediate levels increase and decrease intermittently as expected, while the population of target level $|4\rangle$ reaches one at the final time. The bottom graph shows that the energy of the system increases monotonically from its kinematical minimum value at $t = 0$ to its maximum value at the final time as predicted. The basic response of the system is the same for square wave pulses and Gaussian pulses. However, the energy increases more uniformly for square wave pulses, while Gaussian pulses tend to result in short, steep increases with long intermittent plateau regions. Square wave pulses may therefore be a better choice

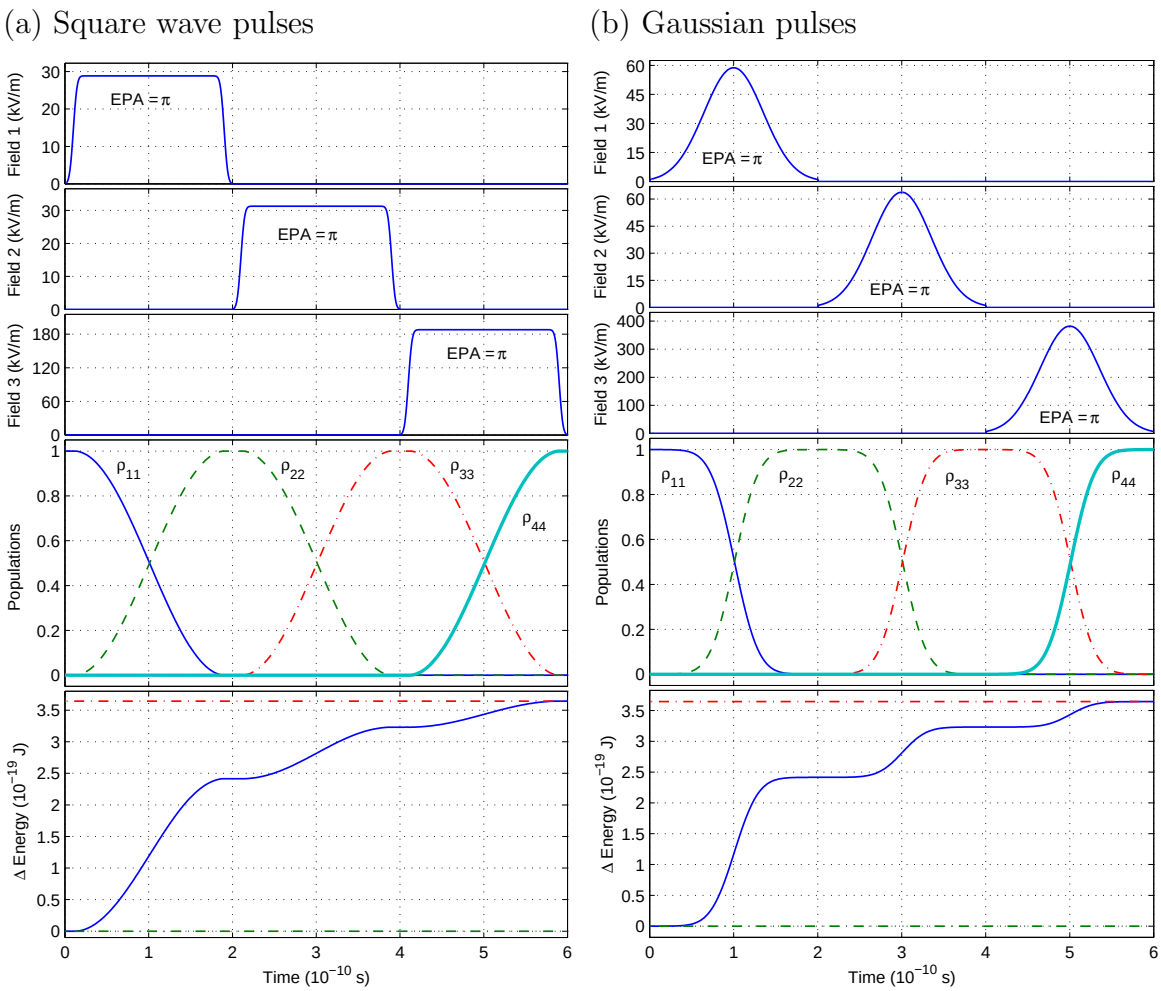

Figure 3. Population transfer from the ground state $|1\rangle = |5S_{1/2}\rangle$ to the excited state $|4\rangle = |6P_{3/2}\rangle$ for ^{87}Rb using (a) three 200 ps square wave pulses with rise and decay time $\tau_0 = 20$ ps and (b) three 200 ps Gaussian pulses with $q = 2 \times 10^{10}$ Hz. The top graphs show the pulse envelopes $A_k(t)$. The effective pulse area $\mathrm{EPA} = \int_{\Delta t_m} 2A_m(t)d_m\,dt$ of all pulses is π. The labels 'Field m' indicate that the corresponding pulses are resonant with the frequency ω_m of the transition $|m\rangle \rightarrow |m+1\rangle$.

if one wishes to minimize the time the system spends in intermediate states with short lifetimes. Gaussian wavepackets, on the other hand, have the advantage of minimal frequency dispersion and are thus less likely to induce unwanted off-resonant effects.

As regards the field strengths, note that for 200 ps pulses up to 380 kV/m are required for SWP, and up to 780 kV/m for Gaussian pulses, which corresponds to (peak) intensities $I = \epsilon_0 c E^2$ of up to 40 kW/cm^2 (SWP) and 160 kW/cm^2 (GWP), respectively. Achieving these intensities experimentally with CW lasers is feasible using a combination of sufficiently powerful lasers and beam focusing techniques. Since pulsed laser systems with 1 mJ output for picosecond pulses are common, intensities of up to 10^7 W/cm^2 should be easy to achieve for these systems.

Note that we chose pulses of fixed length 200 ps and allowed the pulse amplitudes to vary. Had we instead fixed the strength of the fields to be $2A_k = 10^5$ V/m, say, then the length Δt_k of the control pulses according to (26) would have been 124.2, 132.7 and 697.1 ps, respectively, for SWP with $\tau_0 = 20$ ps. For Gaussian pulses with $q_k = 4/\Delta t_k$, the pulse length according to (32) would have been 235.1, 254.7 and 1528.2 ps, respectively. Thus, instead of 600 ps in both cases, the time required to achieve the control objective would have been 954 ps for SWP and 2018 ps for GWP.

7. Inversion of ensemble populations for a mixed-state system

Sequences of π-pulses similar to the ones derived in the previous section have played an important role in the theory of atomic excitation [52] and have been applied to the problem of vibrational excitation of molecules in both theory [53] and experiment [54]. The decomposition technique is an important tool since it allows us to generalize the intuitive control schemes for population transfer between energy eigenstates to obtain similar schemes for a variety of more complicated problems, as we shall demonstrate now.

The first example we consider is a generalization of the population transfer problem to mixed-state systems. The objective is to achieve a complete inversion of the ensemble populations given an arbitrary initial state of the form (19). This control operation can be regarded as an ensemble–NOT gate for mixed-state systems, not to be confused with other NOT–gates such as the U–NOT gate [55]. Complete inversion of the ensemble populations requires an evolution operator

$$\hat{U} = \begin{pmatrix} 0 & 0 & \cdots & 0 & e^{\mathrm{i}\theta_1} \\ 0 & 0 & \cdots & e^{\mathrm{i}\theta_2} & 0 \\ \vdots & \vdots & & \vdots & \vdots \\ 0 & e^{\mathrm{i}\theta_{N-1}} & \cdots & 0 & 0 \\ e^{\mathrm{i}\theta_N} & 0 & \cdots & 0 & 0 \end{pmatrix}, \tag{37}$$

where the $e^{\mathrm{i}\theta_n}$ are arbitrary phase factors. Assuming as before that each transition between adjacent energy levels can be individually addressed, the generators of the dynamical Lie algebra are again of the form (15) and the target operator (37) can be written as a product of these generators

$$\hat{U} = \hat{U}_0(T) \prod_{\ell=N-1}^{1} \left[\prod_{m=1}^{\ell} \hat{V}_m \right], \tag{38}$$

where the factors $\hat{V}_m$ are as defined in (36). The decomposition (38) corresponds to a sequence of $K = N(N-1)/2$ pulses in which the kth pulse is resonant with the transition $|\sigma(k)\rangle \to |\sigma(k)+1\rangle$ and has effective pulse area π, where

$$\sigma([1,\ldots,K]) = [1,2,\cdots,N-1;1,2\cdots N-2;1,2,\cdots,N-3;\cdots;1,2;1].$$

This pulse scheme does *not* depend on the values of the initial populations, i.e., a complete inversion of the ensemble populations is achieved for any initial ensemble.

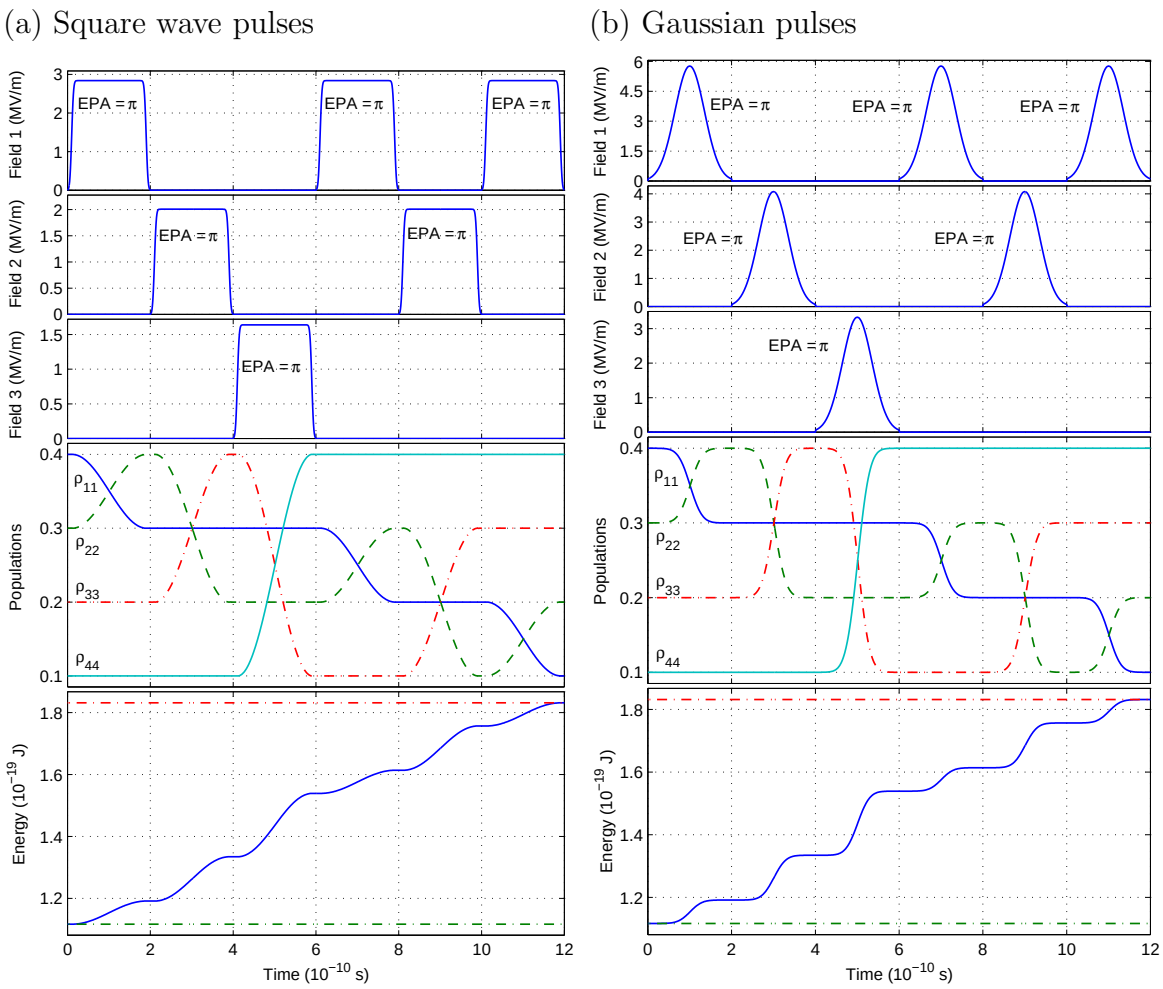

Figure 4. Inversion of the ensemble populations for the vibrational modes of HF using (a) six square wave control pulses with rise and decay time $\tau_0 = 20$ ps, and (b) six Gaussian pulses with $q = 2 \times 10^{10}$ Hz. The top graphs show the pulse envelopes $A_k(t)$. The effective pulse area EPA $= \int_{\Delta t_m} 2A_m(t)d_m\, dt$ of all pulses is π. The labels 'Field m' indicate that the corresponding pulses are resonant with the frequency ω_m of the transition $|m\rangle \to |m+1\rangle$.

Moreover, if the initial populations are mutually distinct, i.e., $w_n \neq w_m$ for $n \neq m$, then the decomposition is optimal in the sense that a complete inversion of the ensemble populations cannot be achieved with fewer than K control pulses.

To illustrate the control scheme, let us apply it to the four-level Morse oscillator model for the vibrational modes of HF discussed above. For the purpose of the computer simulations, we randomly choose the initial populations to be $w_1 = 0.4$, $w_2 = 0.3$, $w_3 = 0.2$ and $w_4 = 0.1$, but recall that any initial ensemble would do, i.e., we could have chosen a thermal ensemble given by a Boltzmann distribution or another ensemble instead. Our goal is to create an ensemble where the populations of the energy eigenstates are reversed, i.e., where $|1\rangle$ has population w_4, $|2\rangle$ has population w_3, $|3\rangle$ has population w_2, and $|4\rangle$ has population w_1.

Figure 4 shows the results of control simulations using square wave and Gaussian control pulses, respectively. Note that each pulse in the control sequence interchanges the populations of two adjacent energy levels until a complete inversion of the populations is achieved. For our four-level system the effect of the controls on the populations can be summarized as follows

$$
\begin{array}{cccccccc}
 & & f_1 & f_2 & f_3 & f_1 & f_2 & f_1 \\
|1\rangle & w_1 & w_2 & w_2 & w_2 & w_3 & w_3 & w_4 \\
|2\rangle & w_2 & w_1 & w_3 & w_3 & w_2 & w_4 & w_3 \\
|3\rangle & w_3 & w_3 & w_1 & w_4 & w_4 & w_2 & w_1 \\
|4\rangle & w_4 & w_4 & w_4 & w_1 & w_1 & w_1 & w_1
\end{array}
$$

where f_m, $m = 1, 2, 3$, refers to a control pulse of frequency ω_m with effective pulse area π. The first pulse interchanges the populations of levels $|1\rangle$ and $|2\rangle$, the second pulse flips the populations of levels $|2\rangle$ and $|3\rangle$, the third pulse switches the populations of levels $|3\rangle$ and $|4\rangle$, etc. Since the populations of our initial ensemble satisfy $w_1 < w_2 < w_3 < w_4$, the energy of the system assumes its kinematical minimum at $t = 0$ and increases monotonically to its kinematical maximum value at the final time. Again, the gradient of approach is more uniform for square wave pulses.

As regards the field strengths, note that for 200 ps pulses up to 5.7 MV/m are required for SWP, and up to 12 MV/m for Gaussian pulses, which corresponds to (peak) intensities $I = \epsilon_0 c E^2$ of up to 8.5 MW/cm^2 (SWP) and 24 MW/cm^2 (GWP), respectively. Achieving these intensities experimentally should be no problem for pulsed laser systems. For CW lasers, it would be challenging at the moment, but it should still be feasible using a combination of powerful lasers and beam focusing techniques. Moreover, such problems should disappear with improvements in laser technology in the future.

Had we instead of fixing the pulse length at 200 ps, fixed the strength of the fields to be $2A_k = 5 \times 10^6$ V/m, say, then the length Δt_k of the control pulses according to (26) would have been 224.5, 164.6, 138.1, 224.5, 164.6 and 224.5 ps, respectively, for SWP with $\tau_0 = 20$ ps. For GWP with $q_k = 4/\Delta t_k$ the pulse lengths according to (32) would have been 461.3, 326.2, 266.3, 461.3, 326.3 and 461.3 ps, respectively. Thus, instead of 1.2 ns in both cases, the time required to achieve the control objective would have been 1.14 ns for SWP, and 2.3 ns for GWP.

Note that the problem of population transfer for a system initially in state $|1\rangle$ is a special case of the problem of population inversion for a trivial ensemble with $w_1 = 1$ and $w_2 = w_3 = w_4 = 0$. It can easily been seen that pulses four, five and six in the pulse sequence above do no harm but have no effect for this initial ensemble

$$
\begin{array}{cccccccc}
 & & f_1 & f_2 & f_3 & f_1 & f_2 & f_1 \\
|1\rangle & 1 & 0 & 0 & 0 & 0 & 0 & 0 \\
|2\rangle & 0 & 1 & 0 & 0 & 0 & 0 & 0 \\
|3\rangle & 0 & 0 & 1 & 0 & 0 & 0 & 1 \\
|4\rangle & 0 & 0 & 0 & 1 & 1 & 1 & 1
\end{array}
$$

and can therefore be omitted. Thus, the general six pulse sequence simplifies in this case to the three pulse sequence in the previous section. This can also be inferred directly from the decomposition (38) of the target operator. For a four level system (38) becomes $\hat{U} = \hat{U}_0(T)\hat{V}_1\hat{V}_2\hat{V}_1\hat{V}_3\hat{V}_2\hat{V}_1$ with $\hat{V}_m$ as in (36). Thus, after applying the pulse sequence the state of the system is

$$\begin{aligned}\hat{\rho} &= \hat{U}_0(T)\hat{V}_1\hat{V}_2\hat{V}_1\hat{V}_3\hat{V}_2\hat{V}_1\hat{\rho}_0[\hat{U}_0(T)\hat{V}_1\hat{V}_2\hat{V}_1\hat{V}_3\hat{V}_2\hat{V}_1]^\dagger \\ &= \hat{U}_0(T)\hat{V}_1\hat{V}_2\hat{V}_1\hat{V}_3\hat{V}_2\hat{V}_1\hat{\rho}_0\hat{V}_1^\dagger\hat{V}_2^\dagger\hat{V}_3^\dagger\hat{V}_1^\dagger\hat{V}_2^\dagger\hat{V}_1^\dagger\hat{U}_0(T)^\dagger.\end{aligned}$$

If $\hat{\rho}_0 = |1\rangle\langle 1|$ then $\hat{V}_3\hat{V}_2\hat{V}_1\hat{\rho}_0\hat{V}_1^\dagger\hat{V}_2^\dagger\hat{V}_3^\dagger = |4\rangle\langle 4|$. Since $\hat{U}_0(T)\hat{V}_1\hat{V}_2\hat{V}_1$ commutes with this operator, the remaining factors cancel in the decomposition

$$\begin{aligned}&\hat{U}_0(T)\hat{V}_1\hat{V}_2\hat{V}_1\hat{V}_3\hat{V}_2\hat{V}_1\hat{\rho}_0\hat{V}_1^\dagger\hat{V}_2^\dagger\hat{V}_3^\dagger\hat{V}_1^\dagger\hat{V}_2^\dagger\hat{V}_1^\dagger\hat{U}_0(T)^\dagger \\ &= \hat{U}_0(T)\hat{V}_1\hat{V}_2\hat{V}_1|4\rangle\langle 4|\hat{V}_1^\dagger\hat{V}_2^\dagger\hat{V}_1^\dagger\hat{U}_0(T)^\dagger \\ &= |4\rangle\langle 4|\hat{U}_0(T)\hat{V}_1\hat{V}_2\hat{V}_1\hat{V}_1^\dagger\hat{V}_2^\dagger\hat{V}_1^\dagger\hat{U}_0(T)^\dagger = |4\rangle\langle 4|\end{aligned}$$

and hence do not change the state of the system.

8. Creation of arbitrary superposition states

In this section we consider the problem of creating arbitrary superposition states from an initial energy eigenstate. Control schemes to create such superposition states may be useful in controlling quantum interference in multi-state systems, and can be considered a generalization of the $\frac{\pi}{2}$ pulses used routinely in free induction-decay experiments [56].

Concretely, assume that the system is initially in the ground state $|1\rangle$. To create the superposition state

$$|\Psi(t)\rangle = \sum_{n=1}^{N} r_n e^{\mathrm{i}\theta_n} e^{\mathrm{i}E_n t/\hbar}|n\rangle = \sum_{n=1}^{N} r_n e^{\mathrm{i}\theta_n}|\tilde{n}(t)\rangle \tag{39}$$

where the coefficients r_n satisfy the normalization condition $\sum_{n=1}^{N} r_n^2 = 1$, we need to find a unitary operator $\hat{U}_I$ such that

$$\hat{U}_I|1\rangle = \sum_{n=1}^{N} r_n e^{\mathrm{i}\theta_n}|n\rangle \tag{40}$$

and decompose $\hat{U}_I$ according to the algorithm described in Appendix B.

To find a unitary operator $\hat{U}_I$ that satisfies (34) we set

$$\hat{W} = \left(\begin{array}{c|c} r_1 & \mathbf{0} \\ \hline r_2 & \\ \vdots & \hat{I}_{N-1} \\ r_N & \end{array}\right), \tag{41}$$

where $\hat{I}_{N-1}$ is the identity matrix in dimension $N-1$, and perform Gram-Schmidt orthonormalization on the columns of $\hat{W}$. This produces a matrix $\hat{U}_1$ which is unitary and satisfies $\hat{U}_1|1\rangle = \sum_{n=1}^{N} r_n|n\rangle$. Hence, $\hat{U}_I = \hat{\Theta}\hat{U}_1$ with $\hat{\Theta} = \sum_{n=1}^{N} e^{\mathrm{i}\theta_n}|n\rangle\langle n|$ satisfies (40).

As an example, we consider the problem of creating the superposition state $|\Psi(t)\rangle = \frac{1}{2}\sum_{n=1}^{4}|\tilde{n}(t)\rangle$ for a four-level system initially in state $|1\rangle$. As outlined above, we set

$$\hat{W} = \begin{pmatrix} 1/2 & 0 & 0 & 0 \\ 1/2 & 1 & 0 & 0 \\ 1/2 & 0 & 1 & 0 \\ 1/2 & 0 & 0 & 1 \end{pmatrix}. \tag{42}$$

and perform Gram-Schmidt orthonormalization on the columns of $\hat{W}$, which gives

$$\hat{U}_1 = \begin{pmatrix} 1/2 & -\sqrt{3}/6 & -\sqrt{6}/6 & -\sqrt{2}/2 \\ 1/2 & +\sqrt{3}/2 & 0 & 0 \\ 1/2 & -\sqrt{3}/6 & +\sqrt{6}/3 & 0 \\ 1/2 & -\sqrt{3}/6 & -\sqrt{6}/6 & +\sqrt{2}/2 \end{pmatrix}. \tag{43}$$

Since $\hat{\Theta} = \hat{I}$ we have $\hat{U}_I = \hat{U}_1$ and applying the decomposition algorithm (appendix Appendix B) leads to the factorization $\hat{U}_1 = \hat{V}_5\hat{V}_4\hat{V}_3\hat{V}_2\hat{V}_1$, where the factors are

$$\begin{aligned} \hat{V}_1 &= \exp\left(+C_1\hat{x}_1\right), \quad C_1 = \tfrac{\pi}{3}, \\ \hat{V}_2 &= \exp\left(-C_2\hat{x}_2\right), \quad C_2 = \arctan\left(\sqrt{2}\right) \\ \hat{V}_3 &= \exp\left(+C_3\hat{x}_3\right), \quad C_3 = \tfrac{\pi}{4}, \\ \hat{V}_4 &= \exp\left(+C_4\hat{x}_2\right), \quad C_4 = \tfrac{\pi}{2}, \\ \hat{V}_5 &= \exp\left(-C_5\hat{x}_1\right), \quad C_5 = \tfrac{\pi}{2}. \end{aligned} \tag{44}$$

This decomposition corresponds to the following sequence of five control pulses

$$\begin{aligned} f_1(t) &= A_1(t)e^{i(\omega_1 t+\pi/2)} + \text{c.c.} &&= -2A_1(t)\sin(\omega_1 t) \\ f_2(t) &= A_2(t)e^{i(\omega_2 t-\pi/2)} + \text{c.c.} &&= +2A_2(t)\sin(\omega_2 t) \\ f_3(t) &= A_3(t)e^{i(\omega_3 t+\pi/2)} + \text{c.c.} &&= -2A_3(t)\sin(\omega_3 t) \\ f_4(t) &= A_4(t)e^{i(\omega_2 t+\pi/2)} + \text{c.c.} &&= -2A_4(t)\sin(\omega_2 t) \\ f_5(t) &= A_5(t)e^{i(\omega_1 t-\pi/2)} + \text{c.c.} &&= +2A_5(t)\sin(\omega_1 t) \end{aligned}$$

with pulse areas $\frac{2}{3}\pi$, $2\arctan(\sqrt{2})$, $\frac{1}{2}\pi$, π and π, respectively. Note that only five instead of six pulses are required since the target operator $\hat{U}_1$ has two consecutive zeros in the last column, which implies that one of the six control pulses has zero amplitude and can thus be omitted.

Figure 5 shows the results of a control simulation based on this decomposition of $\hat{U}_1$ for ^{87}Rb using square wave and Gaussian control pulses, respectively. Note that all the populations and the absolute values of all the coherences are 0.25 at the final time — exactly as required for the superposition state $|\Psi(t)\rangle = \frac{1}{2}\sum_{n=1}^{4}|\tilde{n}(t)\rangle$, whose density matrix representation is

$$\hat{\rho}(t) = |\Psi(t)\rangle\langle\Psi(t)| = \frac{1}{4}\begin{pmatrix} 1 & e^{\mathrm{i}\omega_{12}t} & e^{\mathrm{i}\omega_{13}t} & e^{\mathrm{i}\omega_{14}t} \\ e^{-\mathrm{i}\omega_{12}t} & 1 & e^{\mathrm{i}\omega_{23}t} & e^{\mathrm{i}\omega_{24}t} \\ e^{-\mathrm{i}\omega_{13}t} & e^{-\mathrm{i}\omega_{23}t} & 1 & e^{\mathrm{i}\omega_{34}t} \\ e^{-\mathrm{i}\omega_{14}t} & e^{-\mathrm{i}\omega_{24}t} & e^{-\mathrm{i}\omega_{34}t} & 1 \end{pmatrix},$$

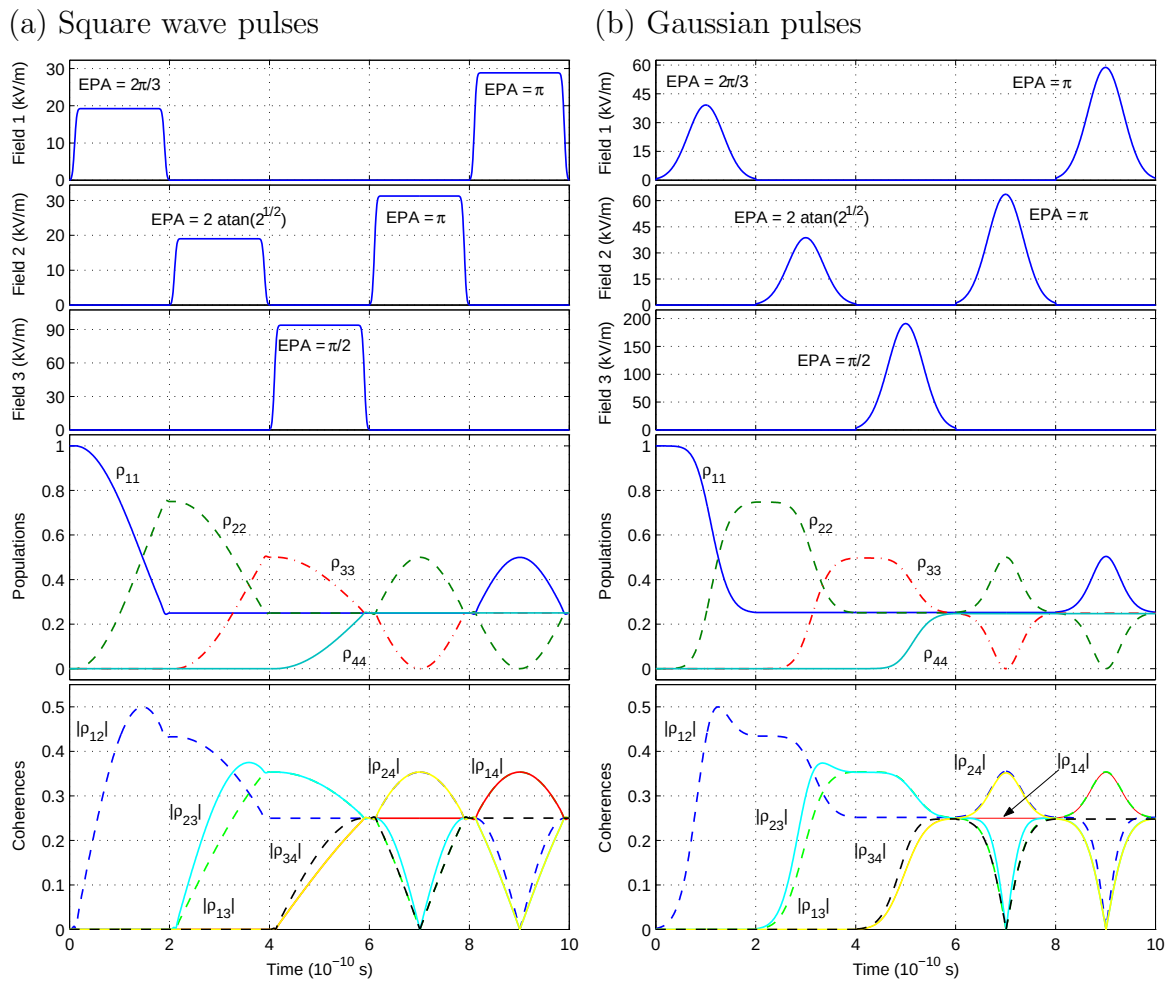

Figure 5. Creation of the superposition state $|\Psi(t)\rangle = \frac{1}{2}\sum_{n=1}^{4} |\tilde{n}(t)\rangle$ for ^{87}Rb initially in the ground state $|1\rangle$ using (a) five 200 ps square wave pulses with rise and decay time $\tau_0 = 20$ ps, and (b) five 200 ps Gaussian pulses with $q = 2 \times 10^{10}$ Hz. The top graphs show the pulse envelopes $A_k(t)$. The effective pulse area (EPA) of all pulses is as shown in the graph. The labels 'Field m' indicate that the corresponding pulses are resonant with the frequency ω_m of the transition $|m\rangle \to |m+1\rangle$.

i.e., $|\hat{\rho}_{mn}| = \frac{1}{4}$ for all m, n. Note that we have plotted the absolute values of the coherences $\hat{\rho}_{mn}(t)$ (for $m \neq n$) only since their phases are rapidly oscillating at frequencies $\omega_{mn} = (E_n - E_m)/\hbar$, which are on the order of 10^{15} Hz for ^{87}Rb. The pulse intensities are similar to those for population transfer in ^{87}Rb. Again, we chose pulses of fixed length 200 ps. Had we instead fixed the strength of the fields to be $2A_k = 10^5$ V/m, say, then the length Δt_k of the control pulses according to (26) and (32) would have been 99.5, 88.6, 358.6, 132.9 and 155.4 ps, respectively, for SWP with $\tau_0 = 20$ ps, and 156.7, 154.9, 764.1, 254.7 and 305.6 ps, respectively, for GWP with $q_k = 4/\Delta t_k$.

Unlike decompositions (35) and (38) where the initial phases ϕ_m of the control pulses were arbitrary, the factorization (44) fixes the pulse area and frequency ω_m as

well as the initial phase ϕ_m of each pulse. In order to determine the significance of the the initial pulse phases on the outcome of the control process, we compute the unitary operator $\hat{U}_2 = \tilde{V}_5\tilde{V}_4\tilde{V}_3\tilde{V}_2\tilde{V}_1$, where the factors are

$$\begin{aligned}
\tilde{V}_1 &= \exp\left[C_1(\sin\phi_1\hat{x}_1 - \cos\phi_1\hat{y}_1)\right] \\
\tilde{V}_2 &= \exp\left[C_2(\sin\phi_2\hat{x}_2 - \cos\phi_2\hat{y}_2)\right] \\
\tilde{V}_3 &= \exp\left[C_3(\sin\phi_3\hat{x}_3 - \cos\phi_3\hat{y}_3)\right] \\
\tilde{V}_4 &= \exp\left[C_4(\sin\phi_4\hat{x}_2 - \cos\phi_4\hat{y}_2)\right] \\
\tilde{V}_5 &= \exp\left[C_5(\sin\phi_5\hat{x}_1 - \cos\phi_5\hat{y}_1)\right]
\end{aligned} \tag{45}$$

and the constants C_k are as in (44) but the initial phases ϕ_k of the control pulses are arbitrary, and apply this operator to the initial state $|1\rangle$. The resulting state

$$\hat{U}_2\begin{pmatrix}1\\0\\0\\0\end{pmatrix} = \frac{1}{2}\begin{pmatrix} e^{\mathrm{i}(\phi_4+\phi_5-\phi_1-\phi_2)} \\ e^{\mathrm{i}(-\pi/2-\phi_5)} \\ e^{\mathrm{i}(\pi-\phi_1-\phi_4)} \\ e^{\mathrm{i}(\pi/2-\phi_1-\phi_2-\phi_3)}\end{pmatrix} \tag{46}$$

differs from the desired target state only in the phase factors, i.e., the pulse phases do not affect the relative amplitudes r_n of the superposition state created. Moreover, we can use (46) to explicitly determine the pulse phases ϕ_n as a function of the phases θ_n of the target state:

$$\begin{aligned}
\phi_1 &= \text{arbitrary} \\
\phi_2 &= \tfrac{\pi}{2} - 2\phi_1 - \theta_1 - \theta_2 - \theta_3 \\
\phi_3 &= \phi_1 + \theta_1 + \theta_2 + \theta_3 - \theta_4 \\
\phi_4 &= \pi - \phi_1 - \theta_3 \\
\phi_5 &= -\tfrac{\pi}{2} - \theta_2.
\end{aligned} \tag{47}$$

Setting $\theta_n = 0$ for $n = 1, 2, 3, 4$ and choosing $\phi_1 = \pi/2$ leads to $\phi_2 = -\pi/2$, $\phi_3 = \pi/2$, $\phi_4 = \pi/2$ and $\phi_5 = -\pi/2$, which agrees with the phases in decomposition (44).

9. Optimization of observables

Finally, we address the problem of maximizing the ensemble average of an observable for a system whose initial state is a statistical ensemble of energy eigenstates (19). Let us first consider the case of a time-independent observable $\hat{A}$. To determine the target operator required to maximize the ensemble average $\langle\hat{A}\rangle$ of $\hat{A}$ we observe that $\langle\hat{A}\rangle$ is bounded above by the kinematical upper bound [57]

$$\langle\hat{A}\rangle \leq \sum_{n=1}^{N} w_{\sigma(n)}\lambda_n, \tag{48}$$

where λ_n are the eigenvalues of $\hat{A}$ counted with multiplicity and ordered in a non-increasing sequence

$$\lambda_1 \geq \lambda_2 \geq \cdots \geq \lambda_N, \tag{49}$$

w_n are the populations of the energy levels E_n of the initial ensemble, and σ is a permutation of $\{1, \ldots, N\}$ such that

$$w_{\sigma(1)} \geq w_{\sigma(2)} \geq \cdots \geq w_{\sigma(N)}. \tag{50}$$

Observe that this universal upper bound for the ensemble average of any observable $\hat{A}$ is dynamically attainable since the systems considered in this paper are completely controllable [58, 59].

Let $|\Psi_n\rangle$ for $1 \leq n \leq N$ denote the normalized eigenstates of $\hat{A}$ satisfying $\hat{A}|\Psi_n\rangle = \lambda_n|\Psi_n\rangle$ and let $\hat{U}_1$ be a unitary transformation such that

$$|\Psi_{\sigma(n)}\rangle = \hat{U}_1|n\rangle, \quad 1 \leq n \leq N. \tag{51}$$

Given an initial state $\hat{\rho}_0$ of the form (19), we have

$$\begin{aligned}
\mathrm{Tr}\left(\hat{A}\hat{U}_1\rho_0\hat{U}_1^\dagger\right) &= \mathrm{Tr}\left(\hat{A}\sum_n w_n\hat{U}_1|n\rangle\langle n|\hat{U}_1^\dagger\right) \\
&= \mathrm{Tr}\left(\sum_n w_n\hat{A}|\Psi_{\sigma(n)}\rangle\langle\Psi_{\sigma(n)}|\right) \\
&= \mathrm{Tr}\left(\sum_n w_n\lambda_{\sigma(n)}|\Psi_{\sigma(n)}\rangle\langle\Psi_{\sigma(n)}|\right) \\
&= \sum_n w_n\lambda_{\sigma(n)} = \sum_n w_{\sigma(n)}\lambda_n.
\end{aligned} \tag{52}$$

Hence, if the system is initially in the state (19) then $\hat{U}_1$ is a target operator for which the observable $\hat{A}$ assumes its kinematical maximum, and we can use the decomposition algorithm described in Appendix B to obtain the required factorization of the operator $\hat{U}_I = \hat{U}_0(T)^\dagger\hat{U}_1$.

However, if $\hat{A}$ is an observable whose eigenstates are not energy eigenstates then the expectation value or ensemble average of $\hat{A}$ will usually oscillate rapidly as a result of the action of the free evolution operator $\hat{U}_0(t)$. These oscillations are rarely significant for the application at hand and often distracting. In such cases it is advantageous to define a dynamic observable

$$\tilde{A}(t) = \hat{U}_0(t)\hat{A}\hat{U}_0(t)^\dagger \tag{53}$$

and optimize its ensemble average instead. To accomplish this, note that if $|\Psi_n\rangle$ are the eigenstates of $\hat{A}$ satisfying $\hat{A}|\Psi_n\rangle = \lambda_n|\Psi_n\rangle$ then $|\tilde{\Psi}_n(t)\rangle = \hat{U}_0(t)|\Psi_n\rangle$ are the corresponding eigenstates of $\tilde{A}(t)$ since

$$\tilde{A}(t)|\tilde{\Psi}_n(t)\rangle = \hat{U}_0(t)\hat{A}\hat{U}_0(t)^\dagger\hat{U}_0(t)|\Psi_n\rangle = \hat{U}_0(t)\lambda_n|\Psi_n\rangle = \lambda_n|\tilde{\Psi}_n(t)\rangle.$$

Hence, if $\hat{U}_1$ is a unitary operator such that equation (51) holds then $\hat{U}_0(t)\hat{U}_1$ is a unitary operator that maps the energy eigenstates $|n\rangle$ onto the $\tilde{A}(t)$-eigenstates $|\tilde{\Psi}_n(t)\rangle$ since

$$\hat{U}_0(t)\hat{U}_1|n\rangle = \hat{U}_0(t)|\Psi_{\sigma(n)}\rangle = |\tilde{\Psi}_{\sigma(n)}(t)\rangle$$

for $1 \leq n \leq N$. Thus, the evolution operator required to maximize the ensemble average of $\tilde{A}(t)$ at time $T > 0$ is $\hat{U}_0(T)\hat{U}_1$ and the target operator to be decomposed is $\hat{U} = \hat{U}_0(T)^\dagger\hat{U}_0(T)\hat{U}_1 = \hat{U}_1$.

For instance, suppose we wish to maximize the ensemble average of the transition dipole moment operator $\tilde{A}(t) = \hat{U}_0(t)\hat{A}\hat{U}_0(t)^\dagger$, where

$$\hat{A} = \sum_{n=1}^{N-1} d_n \left(|n\rangle\langle n+1| + |n+1\rangle\langle n|\right), \tag{54}$$

for a system initially in state (19) with

$$w_1 > w_2 > \cdots > w_N > 0. \tag{55}$$

First, we need to find a unitary operator that maps the initial state $|n\rangle$ onto the $\hat{A}$-eigenstate $|\Psi_n\rangle$ for $1 \le n \le N$. Let $\hat{U}_1$ be the $N \times N$ matrix whose nth column is the normalized $\hat{A}$-eigenstate $|\Psi_n\rangle$. Then $\hat{U}_1$ clearly satisfies $\hat{U}_1|n\rangle = |\Psi_n\rangle$. Furthermore, $\hat{U}_1$ is automatically unitary since the eigenstates $|\Psi_n\rangle$ are orthonormal by hypothesis.

For $N = 4$ and $d_n = p_0\sqrt{n}$ the eigenvalues of the operator $\hat{A}$ defined in (54) are (in decreasing order)

$$\lambda_1 = \sqrt{3+\sqrt{6}},\ \lambda_2 = \sqrt{3-\sqrt{6}},\ \lambda_3 = -\lambda_2,\ \lambda_4 = -\lambda_1$$

and the corresponding eigenstates with respect to the standard basis $|n\rangle$ are the columns of the operator

$$\hat{U}_1 = \begin{bmatrix} \frac{1}{2\lambda_1} & \frac{1}{2\lambda_2} & \frac{1}{2\lambda_2} & \frac{1}{2\lambda_1} \\ \frac{1}{2} & \frac{1}{2} & -\frac{1}{2} & -\frac{1}{2} \\ \frac{\sqrt{2}+\sqrt{3}}{2\lambda_1} & \frac{\sqrt{2}-\sqrt{3}}{2\lambda_2} & \frac{\sqrt{2}-\sqrt{3}}{2\lambda_2} & \frac{\sqrt{2}+\sqrt{3}}{2\lambda_1} \\ \frac{1}{2} & -\frac{1}{2} & \frac{1}{2} & -\frac{1}{2} \end{bmatrix}. \tag{56}$$

Applying the decomposition algorithm described in Appendix B yields the product decomposition $\hat{U}_1\hat{\Theta} = \hat{V}_6\hat{V}_5\hat{V}_4\hat{V}_3\hat{V}_2\hat{V}_1$, where the factors are

$$\begin{aligned}
\hat{V}_1 &= \exp\left(-C_1\hat{x}_1\right), \quad C_1 = \pi/4, \\
\hat{V}_2 &= \exp\left(-C_2\hat{x}_2\right), \quad C_2 = \arctan\left(\sqrt{2}\right), \\
\hat{V}_3 &= \exp\left(-C_3\hat{x}_1\right), \quad C_3 = \operatorname{arccot}\left(\tfrac{\sqrt{6}-\sqrt{3}+3\sqrt{2}}{3}\right), \\
\hat{V}_4 &= \exp\left(-C_4\hat{x}_3\right), \quad C_4 = \pi/3, \\
\hat{V}_5 &= \exp\left(-C_5\hat{x}_2\right), \quad C_5 = \arctan\left(\tfrac{\sqrt{4+\sqrt{6}}}{\sqrt{2}+\sqrt{3}}\right), \\
\hat{V}_6 &= \exp\left(-C_6\hat{x}_1\right), \quad C_5 = \operatorname{arccot}\left(\sqrt{3+\sqrt{6}}\right)
\end{aligned} \tag{57}$$

and $\hat{\Theta} = \mathrm{diag}(1,-1,1,-1)$. Note that $\hat{U}_2 \equiv \hat{U}_1\hat{\Theta}$ is equivalent to $\hat{U}_1$ since $\hat{\Theta}$ commutes with $\hat{\rho}_0$ as defined in equation (19), i.e., $\hat{\Theta}\hat{\rho}_0\hat{\Theta}^\dagger = \hat{\rho}_0$, and thus

$$\mathrm{Tr}\left(\hat{A}\hat{U}_2\hat{\rho}_0\hat{U}_2^\dagger\right) = \mathrm{Tr}\left(\hat{A}\hat{U}_1\hat{\Theta}\hat{\rho}_0\hat{\Theta}^\dagger\hat{U}_1^\dagger\right) = \mathrm{Tr}\left(\hat{A}\hat{U}_1\hat{\rho}_0\hat{U}_1\right). \tag{58}$$

This decomposition corresponds to a sequence of six control pulses

$$\begin{aligned}
f_1(t) &= A_1(t)e^{\mathrm{i}(\omega_1 t-\pi/2)} + \text{c.c.} &&= 2A_1(t)\sin(\omega_1 t) \\
f_2(t) &= A_2(t)e^{\mathrm{i}(\omega_2 t-\pi/2)} + \text{c.c.} &&= 2A_2(t)\sin(\omega_2 t) \\
f_3(t) &= A_3(t)e^{\mathrm{i}(\omega_1 t-\pi/2)} + \text{c.c.} &&= 2A_3(t)\sin(\omega_1 t) \\
f_4(t) &= A_4(t)e^{\mathrm{i}(\omega_3 t-\pi/2)} + \text{c.c.} &&= 2A_4(t)\sin(\omega_3 t) \\
f_5(t) &= A_5(t)e^{\mathrm{i}(\omega_2 t-\pi/2)} + \text{c.c.} &&= 2A_5(t)\sin(\omega_2 t) \\
f_6(t) &= A_6(t)e^{\mathrm{i}(\omega_1 t-\pi/2)} + \text{c.c.} &&= 2A_6(t)\sin(\omega_1 t)
\end{aligned}$$

with effective pulse areas $\frac{\pi}{2}$, $2C_2$, $2C_3$, $\frac{2\pi}{3}$, $2C_5$ and $2C_6$, respectively. Again, the decomposition fixes the frequency and pulse area as well as the initial phase of each pulse and the question thus arises what role the phases play. As we have already seen, the target operator $\hat{U}_1$ is not unique. In fact, equation (58) shows that right multiplication of $\hat{U}_1$ by any unitary matrix that commutes with $\hat{\rho}_0$ produces another unitary operator that leads to the same ensemble average of the target observable. Nevertheless, in general, the control process is sensitive to the phases ϕ_m. For instance, one can verify that changing the phase ϕ_1 of the first pulse from $-\pi/2$ to $\pi/2$ in the pulse sequence above leads to the following evolution operator

$$\hat{U}_3 = \begin{bmatrix} \frac{1}{2\lambda_2} & \frac{1}{2\lambda_1} & \frac{1}{2\lambda_2} & -\frac{1}{2\lambda_1} \\ \frac{1}{2} & \frac{1}{2} & -\frac{1}{2} & \frac{1}{2} \\ \frac{\sqrt{2}-\sqrt{3}}{2\lambda_2} & \frac{\sqrt{2}+\sqrt{3}}{2\lambda_1} & \frac{\sqrt{2}-\sqrt{3}}{2\lambda_2} & \frac{\sqrt{2}+\sqrt{3}}{-2\lambda_1} \\ -\frac{1}{2} & \frac{1}{2} & \frac{1}{2} & \frac{1}{2} \end{bmatrix}, \tag{59}$$

which maps $|3\rangle$ onto $|\Psi_3\rangle$ and $|4\rangle$ onto $-|\Psi_4\rangle$ but $|1\rangle$ onto $|\Psi_2\rangle$ and $|2\rangle$ onto $|\Psi_1\rangle$ and leads to the ensemble average

$$\langle \hat{A} \rangle = w_1\lambda_2 + w_2\lambda_1 + w_3\lambda_3 + w_4\lambda_4 \tag{60}$$

at the final time, which is strictly less than the kinematical maximum if $w_1 > w_2$.

Figure 6 shows the results of control simulations for HF with initial populations $w_1 = 0.4$, $w_2 = 0.3$, $w_3 = 0.2$ and $w_4 = 0.1$ for square wave and Gaussian control pulses, respectively. The pulse intensities are similar to those for population inversion in HF. Notice that the observable indeed attains its kinematical upper bound at the final time, as desired. Furthermore, the target state for which the observable assumes its upper bound is

$$\hat{\rho} = \hat{U}_1\hat{\rho}_0\hat{U}_1^\dagger = \begin{pmatrix} \frac{1}{4} & \rho_{12} & 0 & \rho_{14} \\ \rho_{12}^\dagger & \frac{1}{4} & \rho_{23} & 0 \\ 0 & \rho_{23}^\dagger & \frac{1}{4} & \rho_{34} \\ \rho_{14}^\dagger & 0 & \rho_{34}^\dagger & \frac{1}{4} \end{pmatrix}$$

with $\rho_{12} = \lambda_1\lambda_2(\lambda_2 + \lambda_1/3)/40 \approx 0.0658$, $\rho_{14} = \lambda_1\lambda_2(\lambda_2 - \lambda_1/3)/40 \approx -0.0016$, $\rho_{23} = \lambda_2(\lambda_1^2 - 1/\sqrt{3})/40 \approx 0.0904$, $\rho_{34} = \lambda_2(\lambda_1^2 + 1/\sqrt{3})/40 \approx 0.1118$, which agrees with the final values of the populations and coherences in figure 6. Note that we chose pulses of fixed length 200 ps. Had we instead fixed the strength of the fields to be $2A_k = 5 \times 10^6$ V/m, say, then the length Δt_k of the control pulses according to (26) and (32) would have been 122.2, 97.9, 60.8, 156.3, 82.5 and 72.7 ps, respectively, for SWP with $\tau_0 = 20$ ps, and 230.6, 198.4, 92.2, 307.5, 141.0 and 118.9 ps, respectively, for GWP with $q_k = 4/\Delta t_k$.

10. Conclusion

We have presented several control schemes designed to achieve control objectives ranging from population transfer and inversion of ensemble populations to the creation of

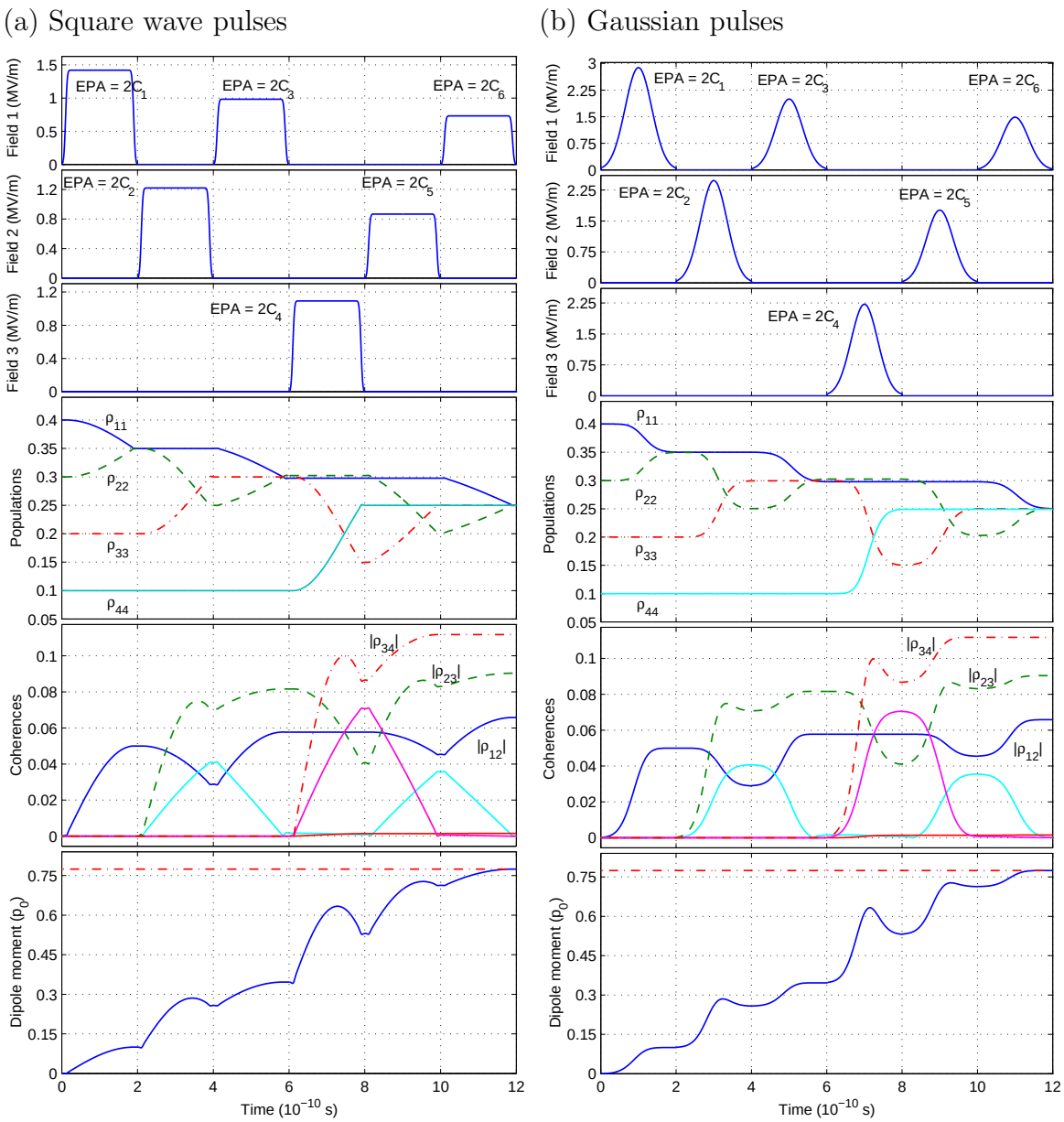

Figure 6. Maximization of the transition dipole moment for HF using (a) six square wave pulses with rise and decay time $\tau_0 = 20$ ps, and (b) six Gaussian pulses with $q = 2 \times 10^{10}$ Hz (right). The top graphs show the pulse envelopes $A_k(t)$. The values of the constants C_k which determine the effective pulse areas (EPA) are given in (57). The labels 'Field m' indicate that the corresponding pulses are resonant with the frequency ω_m of the transition $|m\rangle \to |m+1\rangle$.

arbitrary superposition states and the optimization of (dynamic) observables. A key feature of these schemes is that they rely only on sequences of simple control pulses such as square wave pulses with finite rise and decay times or Gaussian wavepackets to achieve the control objective. In the optical regime, for instance, such pulses can easily be created in the laboratory using pulsed laser sources, or by modulating the amplitude of CW lasers using Pockel cells. No sophisticated pulse shaping technology is required. A limitation of the approach is the need to be able to selectively address individual transitions, which restricts the application of this technique to systems where selection rules and frequency discrimination can be employed to achieve this. However, these requirements can be met for certain atomic or molecular systems, as we have demonstrated for Rubidium and hydrogen fluoride.

Acknowledgements

We sincerely thank A. I. Solomon and A. V. Durrant of the Open University for helpful discussions and suggestions. ADG would like to thank the EPSRC for financial support and VR would like to acknowledge the support of NSF Grant DMS 0072415.

Appendix A. Derivation of equation (10)

Let $\tilde{E}_n = E_n/\hbar$ and $\tilde{d}_n = d_n/\hbar$. Inserting equations (8) and (4) into (9) leads to

$$\begin{aligned}
\mathrm{i}\frac{d\hat{U}_I(t)}{dt} &= \hat{U}_0(t)^\dagger \left\{ \sum_{m=1}^{M} \hat{H}_m[f_m(t)]/\hbar \right\} \hat{U}_0(t)\hat{U}_I(t) \\
&= \sum_{n,m,n'} e^{\mathrm{i}\tilde{E}_n t}\hat{e}_{n,n} A_m(t)\tilde{d}_m \left(e^{\mathrm{i}(\omega_m t+\phi_m)}\hat{e}_{m,m+1} e^{-\mathrm{i}(\omega_m t+\phi_m)}\hat{e}_{m+1,m} \right) e^{-\mathrm{i}\tilde{E}_{n'}t}\hat{e}_{n',n'}\hat{U}_I(t) \\
&= \sum_{m} A_m(t)\tilde{d}_m \left(e^{\mathrm{i}\tilde{E}_m t} e^{\mathrm{i}(\omega_m t+\phi_m)} e^{-\mathrm{i}\tilde{E}_{m+1}t}\hat{e}_{m,m+1} e^{\mathrm{i}\tilde{E}_{m+1}t} e^{-\mathrm{i}(\omega_m t+\phi_m)} e^{-\mathrm{i}\tilde{E}_m t}\hat{e}_{m+1,m} \right) \hat{U}_I(t) \\
&= \sum_{m} A_m(t)\tilde{d}_m \left(e^{\mathrm{i}\phi_m}\hat{e}_{m,m+1} + e^{-\mathrm{i}\phi_m}\hat{e}_{m+1,m} \right) \hat{U}_I(t) \\
&= \sum_{m} A_m(t)\tilde{d}_m \left[\cos\phi_m \left(\hat{e}_{m,m+1} + \hat{e}_{m+1,m} \right) + \mathrm{i}\sin\phi_m \left(\hat{e}_{m,m+1} - \hat{e}_{m+1,m} \right) \right] \hat{U}_I(t) \\
&= \sum_{m} A_m(t)\tilde{d}_m \left(-\mathrm{i}\hat{y}_m \cos\phi_m + \hat{x}_m \mathrm{i}\sin\phi_m \right) \hat{U}_I(t).
\end{aligned}$$

Hence, multiplying both sides by $-\mathrm{i}$ gives

$$\frac{d\hat{U}_I(t)}{dt} = \sum_{m} A_m(t)\tilde{d}_m \left(\hat{x}_m \sin\phi_m - \hat{y}_m \cos\phi_m \right) \hat{U}_I(t). \tag{A.1}$$

Appendix B. Lie group decomposition algorithm

To find a decomposition (16) for the unitary operator $\hat{U}$ we define the equivalent operator $\hat{U}^{(0)} \in SU(N)$ by $\hat{U}^{(0)} = e^{-\mathrm{i}\Gamma/N}\hat{U}$ where $e^{\mathrm{i}\Gamma} = \det(\hat{U})$. Our goal is to reduce $\hat{U}^{(0)}$ step by step to a diagonal matrix whose diagonal elements are arbitrary phase factors $e^{\mathrm{i}\theta_n}$.

Recall that this reduction is always sufficient if the initial state of the system is an ensemble of energy eigenstates.

Let $U_{ij}^{(0)}$ denote the ith row and jth column entry in the matrix representation of $\hat{U}^{(0)}$. In the first step of the decomposition we seek a matrix

$$\hat{W}^{(1)} = \exp\left[-C_1\left(\sin\phi_1\hat{x}_1 - \cos\phi_1\hat{y}_1\right)\right], \tag{B.1}$$

which is the identity matrix everywhere except for a 2×2 block of the form

$$\begin{pmatrix} \cos(C_1) & \mathrm{i}e^{\mathrm{i}\phi_1}\sin(C_1) \\ \mathrm{i}e^{-\mathrm{i}\phi_1}\sin(C_1) & \cos(C_1) \end{pmatrix} \tag{B.2}$$

in the top left corner, such that

$$\hat{W}^{(1)}\begin{pmatrix} U_{1,N}^{(0)} \\ U_{2,N}^{(0)} \\ \vdots \end{pmatrix} = \begin{pmatrix} 0 \\ c \\ \vdots \end{pmatrix} \tag{B.3}$$

where c is some complex number. Noting that $U_{1,N}^{(0)} = r_1 e^{\mathrm{i}\alpha_1}$ and $U_{2,N}^{(0)} = r_2 e^{\mathrm{i}\alpha_2}$, it can easily be verified that setting

$$C_k = -\mathrm{arccot}(-r_2/r_1), \quad \phi_k = \pi/2 + \alpha_1 - \alpha_2 \tag{B.4}$$

achieves (B.3). Next we set $\hat{U}^{(1)} = \hat{W}^{(1)}\hat{U}^{(0)}$ and find $\hat{W}^{(2)}$ of the form

$$\hat{W}^{(2)} = \exp\left[-C_2\left(\sin\phi_2\hat{x}_2 - \cos\phi_2\hat{y}_2\right)\right] \tag{B.5}$$

such that

$$\hat{W}^{(2)}\begin{pmatrix} 0 \\ U_{2,N}^{(1)} \\ U_{3,N}^{(1)} \\ \vdots \end{pmatrix} = \begin{pmatrix} 0 \\ 0 \\ c \\ \vdots \end{pmatrix} \tag{B.6}$$

where c is again some complex number. Repeating this procedure $N-1$ times leads to a matrix $\hat{U}^{(N-1)}$ whose last column is $(0,\ldots,0,e^{\mathrm{i}\theta_N})^T$. Since we are not concerned about the phase factor $e^{\mathrm{i}\theta_N}$ in this paper, we stop here. Note that

$$\exp\left(-C\hat{x}_{N-1}\right) \times \exp\left[-C(\hat{x}_{N-1}\sin\phi - \hat{y}_{N-1}\cos\phi)\right]$$

with $C = \pi/2$ and $\phi = -\pi/2 - \theta_n$ maps $(0, e^{\mathrm{i}\theta_{N-1}})^T$ onto $(0,1)^T$. Hence, a complete reduction to the identity matrix would require two additional steps to eliminate $e^{\mathrm{i}\theta_N}$, which would result in two additional control pulses.

Having reduced the last column, we continue with the $(N-1)$st column in the same fashion, noting that at most $N-2$ steps will be required to reduce the $(N-1)$st column to $(0,\ldots,0,e^{\mathrm{i}\theta_{N-1}},0)^T$ since $\hat{U}^{(0)}$ is unitary. We repeat this procedure until after at most $K = N(N-1)/2$ steps $\hat{U}^{(0)}$ is reduced to a diagonal matrix $\mathrm{diag}(e^{\mathrm{i}\theta_1},\ldots,e^{\mathrm{i}\theta_N})$ and we have

$$\hat{W}^{(K)}\cdots\hat{W}^{(1)}\hat{U}^{(0)} = \mathrm{diag}\left(e^{\mathrm{i}\theta_1},\ldots,e^{\mathrm{i}\theta_N}\right). \tag{B.7}$$

Finally, setting $\hat{V}_k \equiv \left(\hat{W}^{(K+1-k)}\right)^\dagger$ leads to

$$\hat{U}^{(0)} = \hat{V}_K \hat{V}_{K-1} \cdots \hat{V}_1 \mathrm{diag}\left(e^{\mathrm{i}\theta_1}, \ldots, e^{\mathrm{i}\theta_N}\right) \tag{B.8}$$

and therefore $\hat{U} = \hat{V}_K \hat{V}_{K-1} \cdots \hat{V}_1 \Theta$, where $\Theta = e^{\mathrm{i}\Gamma/N} \mathrm{diag}\left(e^{\mathrm{i}\theta_1}, \ldots, e^{\mathrm{i}\theta_N}\right)$ is a diagonal matrix of phase factors.

Recall that $\hat{U}$ can always be decomposed such that Θ is the identity matrix. However, up to $2(N-1)$ additional terms would be required to eliminate the phase factors, which would result in additional control pulses. While some applications indeed require the elimination of these phase factors, they are often insignificant and the additional control pulses would be superfluous. For a more sophisticated decomposition algorithm that requires only very few phases the reader is referred to [60].

References

[1] H. Rabitz, R. de Vivie-Riedle, M. Motzkus, and K. Kompa, Science **288**, 824 (2000).
[2] R. T. Sang *et al.*, Phys. Rev. A **63**, 023408 (2001).
[3] H. Umeda and Y. Fujimura, J. Chem. Phys. **113**, 3510 (2000).
[4] R. J. Levis, G. M. Menkir, and H. Rabitz, Science **292**, 709 (2001).
[5] A. Assion *et al.*, Science **282**, 919 (1998).
[6] R. N. Zare, Science **279**, 1875 (1998).
[7] D. C. Clary, Science **279**, 1879 (1998).
[8] E. Hertz *et al.*, Phys. Rev. A **61**, 033816 (2000).
[9] C. Leonard *et al.*, PCCP Phys. Chem. Chem. Phys. **2**, 1117 (2000).
[10] Y. Zhao and O. Kuhn, J. Phys. Chem. A **104**, 4882 (2000).
[11] D. J. Tannor, R. Kosloff, and A. Bartana, Faraday Discuss. **113**, 365 (1999).
[12] S. G. Schirmer, Phys. Rev. A **63**, 013407 (2001).
[13] G.-L. Long and Y. Sun, quant-ph/0104030 (2001).
[14] A. D. Greentree, S. G. Schirmer, and A. I. Solomon, quant-ph/0103118 (2001).
[15] C. M. Tesch, K. L. Kompa, and R. de Vivie-Riedle, Chem. Phys. Lett. **343**, 633 (2001).
[16] J. Ahn, T. C. Weinacht, and P. H. Bucksbaum, Science **287**, 463 (2000).
[17] C. Ahn, A. C. Doherty, and A. J. Landahl, Phys. Rev. A **65**, 042301 (2002).
[18] N. V. Vitanov, T. Halfmann, B. W. Shore, and K. Bergmann, Ann. Rev. Phys. Chem. **52**, 763 (2001).
[19] V. S. Malinovsky and J. L. Krause, Eur. Phys. J. D. **14**, 147 (2001).
[20] I. R. Sola *et al.*, Phys. Rev. Lett. **85**, 4241 (2000).
[21] B. Y. Chuang *et al.*, J. Chem. Phys. **114**, 8820 (2001).
[22] I. R. Sola, J. Santamaria, and V. S. Malinovsky, Phys. Rev. A **61**, 043413 (2000).
[23] V. S. Malinovsky and J. L. Krause, Phys. Rev. A **63**, 043415 (2000).
[24] W. Zhu and H. Rabitz, J. Chem. Phys. **109**, 385 (1998).
[25] B. M. Goodson, D. Goswami, H. Rabitz, and W. S. Warren, J. Chem. Phys. **112**, 05081 (2000).
[26] W. Zhu and H. Rabitz, J. Chem. Phys. **110**, 7142 (1999).
[27] S. G. Schirmer, M. D. Girardeau, and J. V. Leahy, Phys. Rev. A **61**, 012101 (2000).
[28] Y. Ohtsuki, W. Zhu, and H. Rabitz, J. Chem. Phys. **110**, 9825 (1999).
[29] S. Lloyd, Phys. Rev. A **62**, 022108 (2000).
[30] S. Lloyd and J. J. E. Slotine, Phys. Rev. A **62**, 012307 (2000).
[31] A. C. Doherty *et al.*, Phys. Rev. A **62**, 012105 (2000).
[32] R. J. Nelson, Y. Weinstein, D. Cory, and S. Lloyd, Phys. Rev. Lett. **85**, 3045 (2000).
[33] A. C. Doherty and K. Jacobs, Phys. Rev. A **60**, 2700 (1999).

[34] H. M. Wiseman, Phys. Rev. A **49**, 2133 (1994).
[35] J. M. Geremia, W. Zhu, and H. Rabitz, J. Chem. Phys. **113**, 10841 (2000).
[36] M. Q. Phan and H. Rabitz, J. Chem. Phys. **110**, 34 (1999).
[37] J. Botina and H. Rabitz, Phys. Rev. E **56**, 3854 (1997).
[38] M. Q. Phan and H. Rabitz, Chem. Phys. **217**, 389 (1997).
[39] B. Amstrup *et al.*, J. Phys. Chem. **99**, 5206 (1995).
[40] R. S. Judson and H. Rabitz, Phys. Rev. Lett. **68**, 1500 (1992).
[41] R. Bartels *et al.*, Nature **406**, 164 (2000).
[42] T. Baumert *et al.*, Appl. Phys. B **65**, 779 (1997).
[43] Y. Ohtsuki, H. Kono, and Y. Fujimura, J. Chem. Phys. **109**, 9318 (1998).
[44] B. K. Dey, J. Phys. A **33**, 4643 (2000).
[45] V. Ramakrishna, K. L. Flores, H. Rabitz, and R. Ober, Phys. Rev. A **62**, 053409 (2000).
[46] D. D'Alessandro, in *39th IEEE CDC Proceedings* (Causal Productions, Adelaide, Australia, 2000), pp. 1074–1075.
[47] D. D'Alessandro, in *Proceedings American Control Conference* (Omnipress, Madison, WI, 2001).
[48] F. Albertini and D. D'Alessandro, quant-ph/0106115 (2001).
[49] V. Ramakrishna *et al.*, Phys. Rev. A **61**, 032106 (2000).
[50] N. Weaver, J. Math. Phys. **41**, 5262 (2000).
[51] S. Chelkowski, A. Bandrauk, and P. B. Corkum, Phys. Rev. Lett. **65**, 2355 (1990).
[52] B. W. Shore, *Theory of coherent atomic excitation* (John Wiley & Sons, New York, 1990).
[53] C. M. Tesch, K. L. Kompa, and R. de Vivie-Riedle, Chem. Phys. **267**, 173 (2001).
[54] D. Maas *et al.*, Chem. Phys. Lett. **270**, 45 (1997).
[55] V. Buzek, M. Hillery, and F. Werner, J. Modern Optics **47**, 211 (2000).
[56] A. Abraham, *The Principles of Nuclear Magnetism* (Oxford University Press, London, 1961).
[57] M. D. Girardeau, S. G. Schirmer, J. V. Leahy, and R. M. Koch, Phys. Rev. A **58**, 2684 (1998).
[58] S. G. Schirmer and J. V. Leahy, Phys. Rev. A **63**, 025403 (2001).
[59] S. G. Schirmer, H. Fu, and A. I. Solomon, Phys. Rev. A **63**, 063410 (2001).
[60] V. Ramakrishna, Chem. Phys. **267**, 25 (2001).